Aeolian dust and diatoms at Roosevelt Island (Ross Sea, Antarctica) over the last two millennia reveal the local expression of climate changes and the history of the Ross Sea polynya.

Serena Lagorio[1,2], Barbara Delmonte[1], Dieter Tetzner[3], Elisa Malinverno[1], Giovanni Baccolo[1,4], Barbara Stenni[2], Massimo Frezzotti[4] , Valter Maggi[1], Nancy Bertler[5,6].

[1]University Milano-Bicocca, DISAT – Dept. Earth and Environmental Sciences, Milano, Italy
[2]Ca' Foscari of Venice, Department of Environmental Sciences, Informatics and Statistics, Mestre (Venezia), Italy
[3]BAS, British Antarctic Survey, High Cross, Madingley Road, Cambridge, CB23 7XT, UK
[4]University Roma Tre, Dept. of Sciences, Geological Science Section, Roma, Italy
[5]Antarctic Research Centre, Victoria University of Wellington, Wellington, 6012, New Zealand
[6]GNS Science, National Ice Core Laboratory, Lower Hutt, 5040, New Zealand

Correspondence to: Barbara Delmonte (barbara.delmonte@unimib.it)

Abstract.

The pattern of atmospheric and climate changes recorded by coastal Antarctic ice core sites and the processes they illustrate highlight the importance of multiproxy studies on ice cores drilled from such peripheral areas, where regional to local-scale processes can be documented. Here, we present a 2 kyr long record of aeolian mineral dust and diatoms windblown to the Roosevelt Island, obtained from the RICE (Roosevelt Island Climate Evolution project) ice core. Mineral dust and diatoms are highly complementary at RICE since they are related to the large-scale South Pacific atmospheric circulation regime, carrying dust-rich air masses that travelled above the marine boundary layer, and local oceanic aerosol transport by low-level marine air masses, respectively. The period from 550 to 1470 CE is marked by increased mineral dust transport from Southern Hemisphere continents, a reduction in sea-ice cover in the Eastern Ross and Amundsen Seas, and more frequent incursions of humid air masses, which contributed to a relative rise in snow accumulation. After 1470 CE, relatively lower dust and snow deposition at RICE suggests an increase in pack ice in the Eastern Ross and Amundsen Seas. This period is characterized by prominent peaks of sea ice-related aeolian diatoms that are unprecedented over the last 2 kyr, indicating a rapid reorganization of atmospheric circulation. Data suggests an eastward enlargement of the Ross Sea polynya culminating with the opening of the proposed Roosevelt Island polynya, and an increased influence of low-level marine air masses to the site during the Little Ice Age.

1. Introduction

The assessment of climatic and environmental variability over the Common Era (CE, the last 2000 years before present; 2 kyr BP) is fundamental to place industrial-era warming into the context of natural climatic variability (e.g. IPCC 2021, Smerdon & Pollack, 2016). Based on palaeoclimatic records from Europe, North America and from the extratropical Northern Hemisphere, several climatic periods have been defined and investigated within the past 2 kyr. These include, for example, the so-called "Roman Warm Period" (ca. 1-300 CE, Ljungqvist, 2010) and the "Dark Ages Cold Period" (ca. 400-765 CE, Helama et al., 2017) during the first millennium of the CE. The last millennium is characterized by the "Medieval Warm Period" (MWP), also known as "Medieval Climate Anomaly" (MCA) typically associated with warm temperatures between about 800 and 1200 CE (Lamb, 1965; Mann et al., 2009; Bradley et al., 2003). The most prominent episode that occurred during the last 2 kyr is probably the "Little Ice Age" (LIA), due to its centuries-long cold climate state leading to glacial advances in many locations worldwide (Matthews & Briffa, 2005). The timing and duration of the LIA, however, cannot be precisely defined since the timing, magnitude and regional expression of the LIA exhibit strong regional variations (Jones and Mann, 2004). The post-industrial period (1850 CE-present) is the last of these periods; it is largely recognized to be the warmest period of the past two millennia and to have a strong anthropogenic influence (IPCC, 2021).

The most pronounced characteristic of the anthropogenic warming is its global reach. Conversely, earlier climate swings of the preindustrial CE lack spatial and temporal coherence, and did not produce globally-synchronous temperature changes at multidecadal and centennial timescales (PAGES2k Consortium, 2017). At the scale of the Antarctic continent, a comprehensive ice core-based analysis of climate variability over the last 2000 years (Stenni et al., 2017) highlights a very complex picture with marked differences in regional trends. As an example, the cooling trend registered prior to 1900 CE at sites such as WAIS Divide and in the region of Victoria Land is in apparent disagreement with the water stable isotope record from coastal, low-elevation sites such as Roosevelt Island, located in between the two (fig. 1). There, increasing rather than decreasing water stable isotope anomalies are registered over that period (Bertler et al., 2018). The origin of such differences arises from the intrinsic sensitivity of coastal sites to register regional-to-local atmospheric signals that are often deeply influenced by maritime air masses. The marine influence, by masking longer-term regional temperature trends, enables the capture of high-resolution records of regional and subregional atmospheric variability, which provide a sensitive reflection of the climate and environmental history of the Southern Ocean (Masson et al., 2000; Stenni et al., 2017; Bertler et al., 2018).

In this work, we present and discuss new records of aeolian dust and diatoms obtained from the RICE (Roosevelt Island Climate Evolution project) ice core for the last 2 kyr, providing an excellent opportunity to assess the climate and the atmospheric processes occurring in the Eastern Ross Sea (ERS, the region within the Ross Sea that stretches towards West Antarctica) over the last two millennia. We address three specific questions: (1) What can mineral dust and windblown diatoms tell us about climatic and atmospheric conditions experienced on Roosevelt Island over the last 2 kyr? (2) What climatic and environmental conditions did RICE experience during the last millennium, in particular during the MCA and LIA? (3) How

do the diatom and dust records fit into the wider Ross Sea context? By defining the local expression of climate swings that occurred at RICE and the way they are connected to other local/regional changes, we aim to provide comprehensive insights of the recent climate evolution in the Ross Sea area, regional sea-ice variability and Ross Sea polynya dynamics, as well as air mass circulation driven by large-scale climatic drivers.

1.1 Insoluble impurities in the context of Roosevelt Island

1.1.1 Mineral dust

The RICE ice core, with its relatively high snow accumulation rate of approximately 25±2 cm water equivalent per year over the past 2700 years (Winstrup et al., 2019), offers a unique opportunity to study the coastal Eastern Ross Sea (ERS) and examine the response of regional atmospheric circulation to major climatic drivers, especially in comparison to sites on the East Antarctic Plateau. Indeed, the Ross Sea region is known to be influenced by dynamics affecting both West and East Antarctica, and by oceanic processes (Bertler et al., 2018).

Insoluble impurities found in the RICE ice core mainly consist of mineral dust particles, sourced from New Zealand, southern South America and Australia (Neff & Bertler, 2015). Exposed ice-free areas of West Antarctica also contribute to the dust input at RICE, as deduced by Winton et al. (2016a) based on mineral dust geochemistry and grain size. Although in most East Antarctic sites the concentration of dissolved calcium ions can be used as proxy for a terrestrial source (e.g. Wolff et al., 2010), at RICE the soluble calcium comes primarily from a marine source during the Holocene, and therefore other elements of typical crustal origin such as iron (Fe), aluminum (Al) and manganese (Mn) are better indicators for dust input at the site (Tuohy et al., 2015; Winstrup et al., 2019). The analysis of these elements showed that the seasonal dust pattern is synchronous with black carbon, with a slight tendency to peak in austral summer (Tuohy et al., 2015). However, the annual variability of the dust concentration signal (and related elements) in the snow is quite complex because it is related to three basic and independent factors: (1) atmospheric transport, (2) the availability of fine particles at the dust source and (3) the depositional regime (Delmonte et al., 2017). Crustal elements, such as Fe and Al, tend to display one or two intra-annual peaks at RICE, generally occurring in early-to-late austral winter, while Mn generally peaks in early austral summer, demonstrating that the timing of intra-annual peaks is not always consistent among dust-related elements (Tuohy et al., 2015).

Based on elemental analyses from snow pits, Tuohy et al. (2015) observed a negative correlation between crustal elements and snow density at RICE, suggesting that the highest dust concentration levels can be generally associated with large precipitation related to storm events. It follows from this evidence that dust is deposited at Roosevelt Island mostly through wet deposition during snowfalls. However, the concentration of insoluble particulate material between 1 and 10 μm at RICE obtained from a 2-year snowpit (2011-2012 CE, Winton et al., 2016b) shows that dust deposition in the snow pit is episodic, with two annual impurity maxima corresponding to austral spring-summer, while the lowest dust levels are observed in austral winter months. Again, the scenario appears complex because episodic dust events have also been observed in austral winter (Winton et al.,

2016b). In Antarctica, austral spring-summer dust maxima and austral winter dust concentration minima have been observed at GV7, (Caiazzo et al., 2017), at Berkner Island, that is an ice rise surrounded by the Filchner-Ronne Ice Shelf on the Atlantic sector (Bory et al., 2010), and at South Pole (Legrand and Kirchner, 1988) (fig. 1).

1.1.2 Aeolian diatoms

Although windblown mineral dust aerosol quantitatively represents the most important component of insoluble impurities archived in ice and snow (Delmonte et al., 2013), a quantitatively small but critical fraction of insoluble impurities is represented by other materials, among which are diatoms. Diatoms are single-celled algae (Bacillariophyta) generally light and aerodynamic and thus easily transportable over long-distances by winds (Allen et al., 2020). Diatoms live and prosper in different marine, nonmarine and brackish environments all around the world. When the degree of preservation of individual specimens allows recognizing some species-specific characteristics, the species identification is possible and can aid in identifying potential source regions. Once the source environment is identified, aeolian diatoms preserved in ice core layers can be used as proxy for atmospheric transport pathways complementary to mineral dust (Kellogg & Kellogg, 2005; Burckle et al., 1988). Atmospheric circulation allows a continuous transport of diatoms across Antarctica. However, diatom sources, transport and deposition mechanisms may be geographically different. This implies that the paleoenvironmental significance of the diatom record is different from one glaciological context to another. As an example, in remote high-altitude East Antarctic locations such as Dome C, Vostok (Burckle et al., 1988) and Dome B (Delmonte et al., 2017), the aeolian diatoms allowed to reassess the role of the Patagonian continental shelf at the time of sea level low stand during the last glacial period (Delmonte et al., 2017). This is because the most important diatom sources in these isolated remote sites are the exposed diatom-bearing terrestrial sediments containing marine and nonmarine diatoms (Burckle et al., 1988). In other East Antarctic locations such as Talos Dome for example, located on the periphery of the Antarctic Plateau close to the Transantarctic Mountains (Delmonte et al., 2013), aeolian diatoms mainly derive from reworked subaerially-exposed sediments. Indeed, diatom frustules represent a pervasive component of Antarctic sediments in Victoria Land even at altitude above 2000 m a.s.l. (McKay et al., 2008), and they can be easily remobilized by winds from exposed sediments or subaerially-exposed dry source beds. In South Pole ice, marine and nonmarine species have been observed (Kellogg & Kellogg, 2005). As the surface Antarctic wind field is dominated by katabatic outflow towards the sea with occasional large storm penetration (Bromwich and Robasky 1993), marine diatoms are believed to be carried by these episodic events. A systematic study of diatom concentration in the South Pole ice core over the last 2 kyr revealed that the concentration of diatoms varied between 0 and >450 valves per Liter, and their variability was related to climate conditions with the highest abundances mainly occurring during the LIA (1400-1750 CE) (Kellogg & Kellogg, 1996). More recently, Tetzner et al. (2022a, 2022b) showed through a multi-site approach that diatom species and their seasonal variability vary between coastal, low elevation sites and continental, high elevation sites of the Antarctic Peninsula. While the former display a marked seasonal signal dominated by species like *Fragilariopsis cylindrus* and *Fragilariopsis curta,* typically sourced from the Southern Ocean seasonal sea-ice zone, the latter display a higher

proportion of open ocean diatoms that are more distally-sourced and lack of a clear seasonality. Thus, the authors proposed that the geographically and temporally-variable diatom signal preserved in ice and snow samples from the Antarctic peninsula can be exploited to recover significant environmental information from both the sea-ice zone and the open ocean. In this context, the presence of polynyas, that are areas of open water surrounded by sea ice, can play a major role. This is because polynyas are regions of enhanced oceanic primary and secondary productivity where the growth of phytoplankton biomass, including diatoms, is greater than in adjacent waters (Park et al., 2018).

The Ross Sea wind-driven latent heat polynya is the largest regularly forming polynya around Antarctica. It waxes and wanes between May and October, but mostly develops from early austral spring, until reaching the frontal sea ice margin by January (Arrigo and van Dijken, 2003). In the Ross Sea polynya, phytoplankton blooms peak in early austral summer, declining afterwards in the late austral summer season prior to refreezing (Arrigo and van Dijken, 2003). With an average winter area around $20.23*10^3$ km^2 becoming about $396.5*10^3$ km^2 in austral summer (Arrigo and Van Dijken, 2003), the polynya of the Ross Sea plays an important role in sea ice production, as older sea ice is continually blown offshore and replaced by newly-formed frazil ice.

1.2 Stable water isotopes and snow accumulation at RICE

The ice core stable water isotope record at Antarctic coastal sites is typically sensitive not only to precipitation temperature but also atmospheric circulation and sea ice extent (Bertler et al., 2018). Bertler et al. (2018) provides evidence that the deuterium record at RICE is positively correlated with surface air temperature at the site which, in turn, is representative of surface air temperature variability of air masses across the Ross Ice Shelf and Ross-Amundsen Sea, as well as Western Marie Byrd Land. While the Siple Dome site (fig. 1) is within the area of statistically-significant temperature correlation with RICE, that is not the case for WAIS Divide. Also, there is no correlation between RICE surface air temperature and the westernmost margin of the Transantarctic Mountains.

The δD stable water isotope composition of RICE snow layers is also negatively correlated with sea-ice concentration (SIC) in the Eastern Ross Sea (ERS) and Northern Amundsen Sea (AS), suggesting that less depleted isotope values reflect air mass and humidity advection from the nearby Ross Sea region at times of reduced sea ice (Emanuelsson, 2016, 2018; Bertler et al., 2018). Conversely, isotopically-depleted precipitation might occur at times of expanded sea ice, and/or when air masses travel across West Antarctica before reaching RICE. Sea ice in the ERS/Northern AS also influences snow accumulation rate at RICE, so that periods of reduced (increased) SIC are related to increased (reduced) snow accumulation and isotopically-enriched (depleted) water vapor (Emanuelsson et al., 2023).

At RICE and in the wider Ross Sea region, most of the snow accumulation occurs as snowfall, while clear sky precipitation (diamond dust) represents only a minor contributor (Sinclair et al., 2010). Intense snow accumulation episodes typically occur in correspondence to the western flank of blocking anticyclones, when strong meridional (poleward) winds create a corridor drawing isotopically-enriched air masses from the nearby open ocean, north of the sea-ice edge, to RICE (Emanuelsson et al.,

2018, 2023). Modern meteorological data highlight that these intense precipitation events related to blocking anticyclones are responsible for the N-NE winds that prevail at Roosevelt Island. Currently, blocking events occur in a small percentage of time (ca. 12% in the 1979-2014 CE period) but they are responsible for the largest fraction of the annual precipitation at the site (ca. 88%, Emanuelsson et al., 2016). Interestingly, in relation to these large precipitation and extreme surface air temperature events, a "dipole" pattern in temperature, snowfall and sea ice is generated between the ERS and the Western Ross Sea (WRS), and also between the ERS and the Antarctic Peninsula. By interacting with the eastern flank of low-pressure cells centred over the Ross Sea, the blocking anticyclonic events contribute significantly to the antiphase East-West Ross Sea dipole formation (Emanuelsson et al., 2018).

2. Methods

2.1 The RICE ice core

The RICE ice core was drilled on the NE edge of the Ross Ice Shelf, at the summit of Roosevelt Island (79.364°S, 161.706°W, 550 m a.s.l., fig. 1), an ice rise 764 m thick, locally-grounded 214 m below sea level (Bertler et al., 2018; Lee et al., 2020). At RICE, ice accumulates locally, while the floating ice shelf flows around it. In cross section, the RICE surface topography appears quasi-parabolic with flank slopes extending from a blunt peak (Kingslake et al., 2014). The very low horizontal ice flow coupled to local snow accumulation made this site suitable to extract an ice core drilled to bedrock. To date, the main record is estimated to span 83 kyr, providing rich insights of coastal Antarctic climate (Bertler et al., 2018; Winstrup et al., 2019; Lee et al., 2020). In this study, we focus on the top ~300 m of the core, capturing the last 2 kyr, where important climate and atmospheric patterns at the site occurred (Bertler et al. 2018). The RICE ice core samples were cut for dust and diatom analyses at the New Zealand ice core facility in Wellington. Each sample consisted in dome-shape ca. 15 cm long slices (15x35 mm) from the side of the RICE main core (cutting plan: http://www.rice.aq/core-processing.html).

2.2 Dust analyses

After shipment to Italy, a set of 412 samples spanning the Holocene climate period was measured for dust concentration and grain size at EUROCOLD Laboratory of Milano-Bicocca University. Dust analyses were performed inside a clean room following standard protocols (Delmonte et al., 2017), using Beckman Coulter Multisizers 4 and 4e, both equipped with orifice tubes having an opening of 30 μm. A rigorous intercalibration between the two instruments was implemented prior to the measurements. This setup allows detection of insoluble impurities with equivalent spherical diameter between 600 nm and 18 μm. Within this interval, from the dust size distribution spectra that are defined over 400 channels (log scale), the size distribution indexes of fine particles percent (FPP%) and coarse particle percent (CPP%) were calculated (Delmonte et al. 2017, 2020). Dust mass was calculated from volume-size distribution spectra assuming an average mineral density of 2.5 g/cm^3 (Delmonte et al., 2020).

200

2.3 Diatom analyses

After completion of the dust analyses, residual meltwater aliquots of 10 mL each were filtered on polycarbonate track-etched Isopore™ membranes with a porosity of 0.22 µm. These were mounted on glass slides and observed through a reflected light optical microscope (Olympus BX51M, magnification 100x, 500x, 1000x) in search for diatom valves and fragments. Each valve was identified and counted, then photographed (1000x) and measured for its apical and transapical axis length using the *OLYMPUS Stream Essentials* software. We note that the optical microscope-based approach used in this study is different from former literature works (Tetzner et al., 2022a, 2022b) where scanning electron microscopy (SEM) imaging was used for diatom counting and identification. Thus, in order to estimate the potential counting errors, we compared both methods using a set of 10 samples selected from different depths along the core (from 48 to 625 m depth).

3. Results

The stable water isotope and snow accumulation record from RICE (Bertler et al., 2018) are reported in figure 2a and 2b, respectively, along with the mineral dust size and concentration profile (fig. 2c). This latter shows a pronounced variability (CV ~75% on average) during the last 2 kyr, with a mean of about 16.3 ppb (i.e. ng_{dust}/g_{ice}). For particles smaller than 5 µm in diameter, concentrations are lower than 30 ppb for 90% of the time over the last 2 kyr. Given an average snow accumulation rate at RICE (Bertler et al., 2018) of about 25 cm w.eq. per year (fig. 2b, data from Winstrup et al., 2019), the average dust flux for particles smaller than about 5 µm can be estimated around 4.2 ±3.8 mg m^{-2} yr^{-1} (fig. SF1). This estimate is in line with the flux of ca. 4 mg m^{-2} yr^{-1} calculated for the WAIS ice core site over the last 2.4 kyr (Koffman et al., 2014, fig. SF1). Such fluxes are about a factor ~2-3 higher than those calculated for peripheral East Antarctic high-elevation sites (e.g. Talos Dome and EPICA-DML). Also, they exceed by a factor ~20 the Holocene dust fluxes calculated for inner East Antarctic plateau sites such as Vostok, Dome C and Dome B (Delmonte et al., 2020). Dust size data from RICE also show a degree of particle sorting that is different from central East Antarctic plateau sites (fig. SF2). Indeed, the FPP% and CPP% parameters span a much broader range interval at RICE (20-80% and 10-50% respectively) with respect to plateau sites (30-55% and 10-30%, respectively), as shown in figure SF2.

The decadally-smoothed profiles of dust size and concentration over the last 2 kyr are reported in fig. 2c, along with their long-term smoothing to appreciate variability of the records. Dust concentration is expressed in log-scale, as recommended (Petit & Delmonte, 2009) in order to appreciate the variability of dust background.

Overall, there is no correlation between snow accumulation and particle concentration neither for particles smaller than 10 µm (fig. SF3a) nor for those below 5 µm (fig. SF3b). There is also lack of correlation between snow accumulation and dust grain size (fig. SF3c). Conversely, good agreement exists between dust concentration (flux) and dust grain size, as confirmed by the

Pearson Product Moment Correlation between the variables (fig. SF3d, SF3e) . This means that the major dust inputs are related to fine particle advection.

Both the dust size and concentration records highlight a long-standing period of relatively high dust input starting around 550-600 CE and ending around 1470-1500 CE (fig. 2c), that was qualitatively deduced based on visual inspection of the record. The beginning and the end of this period broadly coincide with the two-step changes of δD (fig. 2a), identified at 580 CE ±27 years and 1477 CE ±10 years by Bertler et al. (2018) using a minimum threshold parameterisation to achieve a minimised residual error. However, we note that a detailed comparison between dust and stable isotope records in terms of leads and lags of changes is limited by the very different sampling resolution of the two records. In correspondence to the period from about 550 CE to about 1470 CE, when the stable water isotope record shows an increase of 3‰, the dust record shows concentrations (and fluxes) higher than average for more than 50% of time, while during the following period from 1470 CE to about 1900 CE, when the stable isotope increases again of 5‰, the dust levels sharply drop to relatively low levels, remaining below average for about 88% of time. The relative difference of dust concentration and fluxes between the three periods 0-550 CE, 550-1500 CE and 1500-1900 CE can be better appreciated from boxplot graphs (fig. SF4). These two latter periods, that are of particular interest to this study, proved to have statistically-significant differences in dust concentration and fluxes on the basis of t-test statistics (supplementary material, fig. SF4).

The stratigraphic record of aeolian diatoms from the RICE ice core is shown in fig. 2d as well as in fig. SF5 (b to e). Both the absolute valve and the valve fragment abundance from this study were normalized considering the time period represented by each sample, spanning ~0.6 to ~2.5 years, in agreement with former studies (Tetzner et al., 2021). The diatom record shows a background influx in the order of 180 valves per Liter per year (valves L^{-1} yr^{-1}) before about 1500 CE, with two minor increases of up to about 2000 valves L^{-1} yr^{-1} around 1200 CE. After the ~1470 CE event of drastic dust decrease and increase in the stable water isotope values, two prominent diatom peaks appear. These peaks exceed 4000 valves L^{-1} yr^{-1} and are unprecedented over the last 2 kyr (fig. 2d, SF5). Diatom peaks are particularly prominent in the periods 1530-1610 CE and 1700-1830 CE for all three indicators - absolute diatom concentration, diatom flux and number of valve fragments detected in the samples (fig. SF5). As diatom concentration and flux data are not lognormally-distributed, the nonparametric Mann-Whitney Rank Sum Test was used as statistic tool to compare the total valve concentration and flux between 1500-1900 CE and the earlier period (0-1500 CE). Results confirm that the difference in the median values between the two groups is greater than would be expected by chance, i.e. there is a statistically significant difference between the two periods.

Regarding diatom analysis, a comparison between optical and electron microscopy revealed that out of a total of 184 valves and 84 fragments, only 2 valves and 16 fragments were missed using the optical method (fig. SF6). Therefore, we estimate that the optical-based diatom abundances reported in this study may be underestimated by approximately 1% for valves and 19% for fragments compared to the SEM-based analysis. The higher percentage for fragments may be due to their smaller

size, which makes them more challenging to identify. Overall, we conclude that the optical-based method used for diatom counting in this study is as reliable as the SEM analysis.

While entire valves could be identified to the species level, this was not the case for most diatom fragments. More than 98.5% of diatom valves were Fragilariopsis spp. (fig 3), which we consider as a unique group. In particular, we observed *F. nana* and *F. cylindrus*, with occasional presence of *F. curta* (fig. 3). Sporadically, doublets of two *F. cylindrus* valves (i.e. pairs of diatom valves attached to one another, forming the simplest colony structure) were detected (fig. 3d), in particular in the most recent section of the record (fig. 2d). Results from morphometric measurements of entire valves oriented in valve view on the filters (fig. 4) show that about 95% of valves display apical axis between 3.4 and 11 µm (mode ~5.3 µm) and transapical axis between 1 and 3.5 µm (mode ~2.2 µm). These data highlight that most diatoms are small-sized, with dimensions similar to those of *F. nana* and *F. cylindrus*, which are similar to the size of mineral dust at RICE (Winton et al., 2016b). As a result, this dimensional similarity makes it challenging to use filtration techniques to separate dust from diatoms, or to apply deep neural networks for identifying diatoms within the samples (Maffezzoli et al., 2023).

4. Discussion

4.1 Transport of dust and diatoms to RICE

The influx of mineral dust aerosols onto the Antarctic ice sheet shows significant variation across space and altitude, as highlighted by the pronounced dust flux gradients in both East and West Antarctica (fig. SF1). The central East Antarctic plateau is mainly impacted by well-sorted dust of remote origin, characterized by low flux values and small dust grains. In contrast, West Antarctica (Koffman et al., 2014) and peripheral Antarctic ice sheet sites (Delmonte et al., 2013; Bory et al., 2010) experience a mix of local and remote dust sources, with a different atmospheric transport regime than plateau sites (Petit & Delmonte, 2009). In this respect, our new dust data from RICE offers an important addition to the understanding of the dust cycle in coastal, low-elevation sites. The paleoclimatic significance of aeolian dust and diatoms transported to RICE is closely tied to its geographic and glaciological setting. Roosevelt Island is a grounded coastal ice rise at the northeastern margin of the Ross Ice Shelf, deeply influenced by its proximity to the open ocean and its neighbouring sea ice zone. Hence, the transport of terrestrial and marine aerosols to the site is very complex. Back trajectory analyses (5 days) of seasonal airmasses for the period 2006-2012 CE (Tuohy et al., 2015) revealed that austral summer trajectories are dominated by three clusters: one is related to local short-range transport, two others represent long-range transport. One of these long-range clusters consists of the distal oceanic component, driven by low-pressure systems moving across the Southern Ocean. This cluster is responsible for the transport of marine aerosols to the RICE site (Tuohy et al., 2015). The second long-range cluster involves air masses that travel over long distances, passing over the South Pacific landmasses before reaching RICE through the West Antarctic/Amundsen-Bellingshausen Seas (ABS, Tuohy et al., 2015). Since these latter pathways are linked to the significant

transport of heavy metals and dust to RICE, Tuohy et al. (2015) concluded that the transport of mineral dust is closely tied to large-scale atmospheric circulation patterns in the South Pacific sector of the Southern Ocean.

Among atmospheric forcing factors responsible for the modulation of long-range transport of dust, we mention the state of the Amundsen Sea Low (ASL), a climatological low pressure centre in the ABS and Eastern Ross Sea area, which is in turn strongly affected by large-scale atmospheric circulation modes of variability such as the Southern Annular Mode (SAM) and the El Niño-Southern Oscillation (ENSO, Emanuelsson et al., 2023).

The aeolian transport of diatoms at RICE follows instead a different atmospheric pattern. Most diatom species are marine planktonic and sea ice-related, supporting a proximal marine origin of diatom-transporting air masses. This hypothesis is corroborated by the evidence of an exceptionally high degree of valve preservation, sometimes being present as doublets in our record. These fresh-looking aspect of diatoms suggest a rapid transport of the cells directly from the proximal marine source to the RICE ice core site, and support the hypothesis that the main diatom source at the site is represented by the nearby Ross Sea waters.

Previous studies (Allen et al., 2020; Tetzner et al., 2021, 2022a, 2022b) on West Antarctica and the Antarctic Peninsula have shown that diatom species and their seasonal variability can differ between coastal, low-elevation sites and continental, high-elevation sites. Coastal areas exhibit a distinct seasonal signal, dominated by species such as F. *cylindrus* and F. *curta*, which are typically sourced from the seasonal sea ice zone (SSIZ). In contrast, continental sites at higher elevations are enriched with open ocean diatoms from distal sources (Tetzner et al., 2022b). Additionally, the seasonal signal at these higher elevation sites is less pronounced.

In this sense, RICE mostly resembles coastal sites of the Peninsula, where local diatom transport is predominantly related to local oceanic air mass transport. The stratigraphic records of aeolian dust and diatoms at RICE, therefore, are highly complementary since they are related to different types of atmospheric transport. As discussed below, these new records open new perspectives on the interpretation of the paleoclimatic signals from the core.

4.2 Environmental changes at RICE in the context of the Ross Sea region: the period from 0 CE to 1470 CE

The reconstruction of dust and diatom variability at RICE offers a valuable opportunity to explore the influence of key drivers of regional climate conditions over the past two millennia, as well as the major atmospheric and oceanic changes in the Eastern Ross Sea area. Throughout the dust record, we observe that periods of elevated dust concentration and flux are generally associated with finer particles. This suggests that the most significant dust transport events at RICE are linked to the advection of remotely-sourced particles, rather than local transport. Although no statistically significant relationship is found at finer time scales, periods of increased dust input at RICE, including the extended period from 550-1470 CE, which encompasses the Medieval Climate Anomaly (MCA), appear to coincide with higher snow accumulation rates and more enriched stable water isotope values, at least until around 1250-1300 CE. Bertler et al. (2018) found that stable isotopes exhibit a statistically

significant negative correlation with sea-ice extent in the South Pacific (AS/ERS). Therefore, periods of increased dust input generally align with periods of reduced sea-ice extent in the ERS sector of the Southern Ocean, as indicated by higher snow accumulation rates and more enriched stable water isotopes. We conclude that increases in dust, stable isotopes and snow accumulation are associated with reduced sea-ice extent in the ERS and more effective penetration of long-range northerly air masses to the RICE site. Since dust-rich air masses typically travel above the marine boundary layer (Petit & Delmonte, 2009), we do not expect to observe significant input of open ocean marine diatoms together with mineral dust. Indeed, our data indicates that during periods of increased dust content, only background levels of aeolian diatom influx are detected at the site. (fig. 2, fig. SF5).

To put our climate reconstruction at RICE into the broader context of the Ross Sea region, we compare our data with TALDICE ice core records from Talos Dome. This site is located on the periphery of the East Antarctic plateau facing the Ross Sea and the South Pacific (fig.1). The sea-salt sodium (ssNa) record from the site has been interpreted as related to the extent of newly-formed pack ice in the Western part of the Ross Sea. We observe therefore (fig. 5b) that around 800-1000 CE the extent of pack-ice neoformation in the WRS was very low (Mezgec et al., 2017), while it increased from ~1000 CE to 1300 CE. In parallel, we observe that between ~800 and 1000 CE, the Ross Sea "polynya efficiency" index was indeed also quite low, while it increased from about 1000 CE. This polynya-related parameter was introduced by Mezgec et al. (2017) and since it is derived from a stacked marine record of *F. curta* from the coastal sea ice zone of the WRS and from the ssNa record from Taylor Dome, it is mainly linked to the activity of the Ross Sea polynya on its westernmost side.
Interestingly, around 1200-1300 CE, when the RICE snow accumulation reaches its maximum and dust influx remains high (suggesting an efficient marine air mass penetration to the site), the sea ice in the ERS and Amundsen Sea was likely minimum while, conversely, pack-ice extent in the WRS was at its maximum extent. We deduce that the period around 1200-1300 CE was the time when the Ross Sea experienced a strong sea ice dipole between its eastern and western parts (fig. 5 b-c). This time period coincides with maximum expression of the Ross Sea temperature dipole observed from the comparison of stable water isotope records of RICE and TALDICE (Bertler et al., 2018).

4.2.1. The dipole pattern and climate drivers

To accurately interpret our 2 kyr record, it is crucial to consider current meteorological patterns in the Ross Sea as well as the meteorological effects of El Niño and La Niña. The establishment of a "dipole-like" pattern in air temperature and sea-ice concentrations between the ERS and WRS is often associated with formation of near-stationary anticyclones (Emanuelsson, 2018). These impede the progression of the westerly circulation and induce a significant meridional transport to RICE from N-NE (Turner et al. 2016), that is responsible for humidity advection to the site. Indeed, several research studies highlight the importance of the Amundsen Sea Low (ASL) on the climate of the Amundsen–Bellingshausen Sea (ABS)/ERS region, and

hence the climate at Roosevelt Island. The ASL is an area of climatologically low atmospheric pressure characterized by a large geopotential height variability, associated with both depressions and blocking high pressure ridges. When these near-stationary anticyclones form, they impede the progression of the westerly circulation and associated storm tracks. It has been observed (Turner et al., 2013; O'Connor et al., 2021; Raphael et al., 2019; You and Maycock, 2019) that the ASL depth and location, both latitude and longitude, vary in relation to other climate drivers, including El Niño Southern Oscillation (ENSO), Pacific Decadal Oscillation (PDO) and the Southern Annular Mode (SAM). In particular, the frequency of blocking events in the southern high latitudes increases significantly during ENSO warm phases (El Niño), particularly over the southeast Pacific during the austral spring and summer (Renwick, 1998). Observational data provides evidence that El Niño climate conditions induce anomalous northerly wind flow along the western side of the blocking ridge in the Amundsen/ERS. This pattern favours poleward movement of sea ice and net sea ice loss with advection of warm and moist air masses towards the RICE site (Zhang et al., 2021). In addition, reanalysis-forced regional climate model outputs indicate that central Pacific El Niño results in a significant increase in snow accumulation in the western Ross Sea sector, while causing a notable decrease in the Amundsen Sea sector, while an eastern Pacific El Niño is associated with similar, albeit weaker, patterns (Macha et al., 2024).
However, the response to El Niño forcing in the Ross Sea is double-sided: while the eastern part of the Ross Sea displays a statistically-significant negative correlation between the Southern Oscillation Index (SOI) and temperature, with warmer temperatures during El Niño events, the coastal WRS areas of Victoria Land show positive or non-significant correlation with SOI, with generally colder temperatures during El Niño events, southerly winds, surface temperature cooling and lengthening of the sea-ice season (Li et al., 2021). No significant relationship between pack ice in the western part of the Ross Sea and ENSO emerges from modern data, while in the Amundsen and ERS the sea ice decreases by 10-20% during El Niño events and increases in the Eastern Amundsen and Bellingshausen Sea as well as in the Weddell Sea. This pattern is known as the Antarctic sea ice dipole, representing the leading mode of ENSO-related Antarctic Sea ice variability (Li et al., 2021). The reason for the tight coupling between El Niño and atmospheric circulation in the area of RICE and more generally in the Ross Sea (Bertler et al. 2004) relies on changes of the split jet in the proximity of New Zealand. This induces a subsequent weakening of the polar front jet during El Niño, an eastward shift and weakening of ASL, reduced cyclone density in the ERS and more frequent blocking, with associated thermal and mechanical forcing (Bertler et al. 2011).

On longer (climatological) timescales, these considerations suggest a possible relationship between dust input to RICE, local snow accumulation, stable water isotopes, sea ice in the WRS and ENSO. Since ENSO is a complex climate pattern that involves interactions between the ocean and the atmosphere, relying on a single proxy for paleo-ENSO may oversimplify the underlying dynamics, which cannot be fully captured by a single proxy alone. For this reason, in this study we use two widely-recognized and well-established paleo-records to investigate ENSO behaviour over the past 2 kyr. These are the SOI-precipitation (SOIpr) index from the tropical Pacific (Yan et al., 2011, fig. 5d) and the red color intensity record from Laguna Pallcacocha in southern Ecuador (Moy et al., 2002, fig. 5e). The SOIpr index is calculated as the difference between normalized annual rainfall data from the tropical western Pacific and the equatorial eastern and central Pacific (Yan et al., 2011), with

negative values of the index indicating El Niño-dominated conditions. For the past two millennia, precipitation records from Indonesia and the Galápagos Islands were selected for the calculation of the index. Specifically, historic rainfall data for Indonesia were derived from salinity reconstructions based on planktonic foraminifera oxygen isotopes and Mg/Ca ratios, while rainfall history in the Galápagos was reconstructed using lake level data from El Junco (Yan et al., 2011). Indeed the grain size of sediments in El Junco lake (fig 5d) is highly sensitive to precipitation changes associated with the Pacific Walker Circulation and El Niño events. The second ENSO proxy we refer to in this study is based on the colour and composition of sediment layers at the bottom of Laguna Pallcacocha (Ecuador). This is linked to intense El Niño events, since increased convective precipitation driven by anomalously high sea surface temperatures in the Pacific leads to higher stream discharge and increased terrestrial material input into the lake. This detrital input includes iron-rich minerals, typically reddish in colour. As a result, periods of increased or decreased runoff can be detected by analysing the red intensity record of sediment layers, from which a time series of moderate-to-strong El Niño events has been constructed (Moy et al., 2002). Because these two series capture the regional impacts of ENSO events and are based on different proxies, they exhibit both similarities and differences; however, some time intervals where both paleo-ENSO records exhibit dominant El Niño-like conditions over the last 2 kyr can be identified. Taking into account periods when SOIpr index is negative and at the same time the red colour intensity record is above the 75th percentile, as example, some intervals dominated by El Niño-like conditions can be identified. The longest of these is the ~400 years long period from 1000 CE to about 1400 CE, followed by a ca. 80 years long period from ~255 to 335 CE (fig. 5, grey bars). During both these periods, we observe an increase in snow accumulation at RICE, as well as relatively high or increasing dust levels, consistent with the scenario described above of preferential advection of warm and moist air masses to RICE site. On the other hand, the stable isotope signal appears more complex. While it shows an increase in tandem with the dust record as previously discussed, it does not show a discernible peak around 300 CE interval (Fig. 1). This is likely because the earliest part of the RICE record represents a period of dynamic changes in the Ross Ice Shelf, with the calving line either terminating or having just completed its last phase of retreat (Yokoyama et al., 2016). Under these conditions, it can be hypothesized that the surface waters of the Eastern Ross Sea were much cooler, leading to a different response in stable isotopes. We conclude that the variability of snow accumulation and dust flux/concentration align with the relationship expected between El Niño and atmospheric circulation anomalies in the Ross Sea region inferred from present-day meteorological data.

The El Niño-related weakening of the zonal westerly winds in the region between 45°–70°S, 90°–150°W with consequent increase of air mass advection from the N-NE to the RICE site seem to be related to the enhanced meridional flow to the WAIS divide observed by Koffman et al. (2014). By analysing mineral dust size in the WAIS ice core, Koffman et al. (2014) observed a southward shift of the Southern Westerly Winds and increased meridional dust transport to WAIS during El Niño events. Indeed this can result from blocking events in the Eastern Ross Sea (Emanuelsson, 2018), and in this sense, the coherency between our observations and conclusions from Koffman et al. (2014) for WAIS divide can be justified.

Similarly, the shift southwards of south Westerlies in association with El Niño is also imprinted in the marine sediment record GeoB3313-1 from the Chilean continental slope (41°S, 74°27'W). This record is tightly related to the rainfall history of the

western side of the Chilean Andes, and suggests enhanced aridity around 1110–1395 CE (fig 5f) in Southern Chile. As noted by Koffman et al. (2014), this feature is also in agreement with a southern shift of the South Westerly Winds. Interestingly, such a feature is also notable around 300 CE, where El Niño-like conditions are observed, supporting the possible relationship observed in the most recent part of the record.

4.3 The period 1470-1900 CE

After about 1470 CE, the RICE record is characterized by a sudden drop in dust concentration and flux, accompanied by a more gradual snow accumulation decrease suggesting increased pack ice in the ERS/Amundsen Sea. In parallel, the stable water isotope composition at RICE increases abruptly, in apparent contradiction to the general relationship between snow accumulation/sea ice and stable water isotopes observed in the earlier part of the record. Bertler et al. (2018) hypothesized that a novel source for isotopically-enriched vapor could justify this sudden stable water isotope increase. Interestingly, such isotope enrichment during the LIA time frame coincides with the appearance of unprecedented peaks in the concentration of sea ice-related and marine planktonic diatoms (fig. 2, 6, S4). These are predominantly observed between ~1500 CE and 1850 CE as two separate peaks around 1530-1610 CE and 1700-1830 CE.

Diatom peaks occur concurrently with stable water isotope enrichments and decreased snow accumulation. This means they correspond to a period of intense influence of local low-elevation marine air masses originating from the marine boundary layer. This is also suggested by the significant increase of marine species (Na^{+}, Ca^{2+}, K^{+}, Mg^{2+}, $SO4^{2-}$) in the RICE ice core (fig. 6, data from Brightley, 2017) in correspondence to diatom peaks, with respect to the period 1200-1400 CE. Comparable values of aeolian diatom fluxes have never been observed along the RICE record and point towards the presence of newly-exposed oceanic water masses in proximity of the site. We note that the position of the calving line remained almost the same during that period (Yokoyama et al., 2016); therefore, we believe the diatom peaks can be related to a new phase of expansion of the Ross Sea polynya during the sea ice formation season. In particular, we suggest an enlargement of the Ross Sea polynya along the central and eastern portion of the Ross Ice Shelf front, which may imply the opening of the *Roosevelt Island Polynya*, considered as the eastern extension of the significantly larger Ross Sea polynya. This development could have exerted a considerable influence on a regional scale.

4.3.1 Ross Sea polynya formation and associated meteorological patterns

Diatoms windblown to the RICE site likely underwent a very short transport directly from the adjacent sea, as revealed mainly by their excellent degree of preservation. Specimens consist almost exclusively of marine planktonic and sea ice-related species, that we believe to be entrained by winds during the early austral spring, at the time of the rapid increase of the polynya areal extent. The Ross Sea Polynya is considered to be primarily a wind-driven polynya (Zwally et al., 1985) although it may be in part thermally-driven (Jacobs and Comiso, 1989). The enlargement of the polynya, mostly occurring west of the date

line, is mainly related to enhanced katabatic drainage from Byrd, Skelton, and Mulock glaciers, from barrier winds along the Transantarctic Mountains and from katabatic surges originating from the Siple Coast of West Antarctica propagating horizontally across the Ross Ice Shelf to its northern edge (Bromwich et al., 1998, Morales Maqueda et al., 2004). Ice production and drift from the Antarctic Ross Sea polynya is also modulated by a semipermanent low-pressure system located to the east (Bromwich et al., 1998; Drucker et al., 2011). In the Ross Sea, in particular, this low-pressure system produces strong southerly winds off the western Ross Ice Shelf and a return air flow towards Roosevelt Island (Drucker et al., 2011). This return flow is particularly relevant as the potential driver for the atmospheric transport of diatom and marine aerosol to the RICE site from the nearby sea surface waters.

The Holocene history of the Ross Sea polynya activity documented by Mezgec et al. (2017) is mainly based on marine sediment and ice core data from the WRS and from East Antarctica. Thus, it represents a comprehensive picture of the W-NW Ross Sea polynya, where the major enlargement typically occurs, but it is not possible to exclude that the development of the polynya in the central part of the ice shelf front and towards the much smaller Roosevelt Island polynya might have had a slightly different evolution. Present-day data (Wang et al., 2022; Tianjiao et al., 2022) highlight that the eastward expansion of the polynya is generally correlated to the integrated areal expansion of the polynya itself. This evidence could account for the agreement between the diatom peaks in the RICE records during the LIA and the increase in the "polynya efficiency" index (Mezgec et al., 2017). Bromwich et al. (1993) observed that the speed of katabatic surges from the Siple Coast plays a key role in modulating the opening of the polynya in the central part of the Ross Ice Shelf front. It is therefore plausible that the intensity of katabatic surges from the Siple Coast increased during the Little Ice Age (LIA), contributing to a significant expansion of the polynya along the central and eastern parts of the Ross Ice Shelf front. In the context of the present-day climate, enhanced southerly winds off the central Ross Ice Shelf are likely associated with a deeper low-pressure system centred approximately north of RICE. Therefore, this cyclonic circulation system may drive the advection of marine aerosol-rich air masses towards our drilling site.

Meteorological observations highlight that katabatic surges typically promote the establishment and development of mesoscale cyclones inside the Ross Sea. After their formation, they then move north-eastwards, ultimately bringing maritime air masses to the site (Carrasco et al., 2003). Numerical simulations by Heinemann and Klein (2003) show that the topography of Antarctica plays an essential role in mesocyclone formation where the convergence of katabatic airflow provides cyclonic shear for the initial formation of the cyclone. Therefore, katabatic winds are the primary factor driving the opening and development of coastal polynyas. These polynyas, in turn, create an area of open water near the coast, which serves as a source for sensible and latent heat fluxes. This promotes low-level baroclinicity between the open water and the continent, leading to further warming and moistening of the atmosphere over the polynya, which contributes to mesocyclogenesis (Klein and Heinemann, 2001). We propose that there may be a positive feedback between katabatic winds, polynya formation, and the development of mesoscale cyclones. After the initial development, the evolution of mesocyclones requires upper-level synoptic-scale support to form a synoptic or sub-synoptic system (Heinemann and Klein, 2003; Carrasco et al., 2003).

505

4.3.2 Atmospheric conditions leading to enhanced diatom transport during the LIA

Given the above-mentioned meteorological evidence for present-day climate, we hypothesize that during the LIA the local maritime air mass advection towards the RICE site, responsible for diatom and marine aerosol transport to the site, might have
510 been related to increased katabatic winds over the central and Western part of the Ross Ice Shelf with maximum polynya development and enhanced atmospheric return flow of local maritime air masses to RICE (fig. 6 c). We believe that these maritime, diatom-rich air masses derive from low-elevation atmospheric layers. In fact, the dynamical and thermodynamical interactions between atmosphere and ocean are strongly influenced by the presence of the polynya, that modifies the vertical structure of the atmosphere promoting the development of a relatively thicker and well-mixed convective boundary layer
515 (Fusco et al., 2009). We also note that the opening of the Roosevelt Island polynya had influence on local scale, since the sodium record from Siple Dome, located some hundreds of kilometres on the Siple Coast of West Antarctica (Kreutz et al., 1997) mimics the expansion of the whole Ross Sea polynya (fig. 6 a). The hypothesis of a significant enlargement of the Ross Sea polynya during the LIA is also supported by data from the western side of the Ross Sea, pointing towards prolonged cold climate conditions with significant increase of katabatic winds and polynya areal extent between the 16th century and the
520 beginning of the 19th century. The TALDICE ice core shows the most negative stable water isotope values of the last 2000 years (Stenni et al., 2011) and an 11% decrease in snow accumulation compared to the preceding period, indicating colder and windier conditions at that time. Indeed, cooling in East Antarctic and the Ross Sea could lead to stronger katabatic flow, in turn leading to an increased polynya efficiency and more sea-ice production (Mezgec et al. 2017). The Taylor Dome record shows prolonged cold stable water isotope temperature anomalies (Steig et al., 2000), and the stable water isotope and
525 geochemical records from Mt. Erebus Saddle (Rhodes et al., 2012) highlight that the region experienced colder than average temperatures prior to 1850 CE and strong katabatic winds between 1500 and 1800 AD. According to Rhodes et al. (2012), prior to 1875 CE the biological productivity in the Ross Sea polynya was ~80% higher than any subsequent time. Bertler et al. (2011) also report colder temperatures and more extensive sea ice, as well as decreased snow accumulation in the WRS at the time of the LIA. The increased efficiency of the Ross Sea polynya over the last ~500-600 years is also reflected in significant
530 ecological changes in Victoria Land (fig. 6). Hall et al. (2006, 2023) observed the near-complete disappearance of elephant seal (Mirounga leonina) colonies in Victoria Land, which they linked to the increased persistence of landfast sea ice. We note that a key factor for the reproductive success of elephant seals is the proximity of open water to their nursery sites. Thus, the disappearance of elephant seal colonies in Victoria Land during the LIA can be interpreted as being related to a significant increase in landfast sea ice. This hypothesis is also supported by independent marine data, such as those from Edisto Inlet in
535 the north-western Ross Sea (Tesi et al., 2020), where persistent summer fast ice has been observed over the last 700 years.
Given that the formation, persistence, and variability of Antarctic polynyas are known to be influenced by landfast sea ice (Fraser et al., 2019; Mezgec et al., 2017), we hypothesize that our data (Fig. 6) support the connection between the permanent

abandonment of the elephant seal population along the Victoria Land coast during the LIA and the expanded extent and occurrence of the Ross Sea polynya. This relationship was previously proposed by Mezgec et al. (2017) for the Holocene period.

Between about 1470 CE and 1900 CE, a time for which we infer the expansion and development of the Roosevelt Island polynya, predominance of positive SOIpr and enhanced Pacific Walker circulation (Yan et al., 2011) suggest a more La Niña-like mean state. We note that here we use the recent SOIpr hydrological reconstruction that includes records from the Indo-Pacific, from the central tropical Pacific and from the eastern equatorial Pacific and which is an atmospheric/hydrological record in agreement with other hydrological records (Rein et al., 2005) indicating a more La Niña-like mean state during the LIA. However, this series conflicts with sea surface temperature reconstructions that suggested the LIA was characterized by a more El Niño-like state, as discussed in detail by Yan et al. (2011). Under La Niña-like conditions, the polar front jet (Turner, 2013) and the ASL became more intense (deeper ASL), while the low-level easterly jet along with the katabatic flow from the Antarctic are enhanced (Bertler et al., 2006). As a result, a deeper ASL often coincides with a larger Ross Sea polynya, as also revealed (Wang et al., 2022) by modern satellite data.

5. Conclusions

The influx of aeolian dust and diatoms at RICE are related, respectively, to large-scale atmospheric circulation patterns in the ERS/Amundsen Sea and to the local oceanic influence of air masses from the marine boundary layer. The combination of these proxies improves the understanding of the climatic and atmospheric changes experienced by Roosevelt Island over the past 2 kys, that are related to a number of forcing factors such as ENSO. During the 550-1470 CE period, when higher/less depleted stable water isotope values are observed, the increased importance of blocking ridges in the Amundsen Sea and a weakened ASL promoted dust-rich air mass advection to RICE. This pattern was accompanied by an increasing trend in snow accumulation and reduced sea ice in the ERS/Amundsen Sea. Comparison with WRS data suggest an opposite behaviour on the two sides of the Ross Sea around 1200-1300 CE, with enhanced katabatic outflow in the WRS, reactivation of the Ross Sea polynya, and maximum extent of pack ice. Interestingly, sustained multi-decadal El Niño dominating conditions coincide with periods of enhanced northerly air mass advection to RICE and with the southward shift of the South Westerly Winds hypothesized on the basis of data from West Antarctica and South America.

After 1470 CE, the RICE site was subject to a rapid atmospheric circulation reorganization in response to the development of the Roosevelt Island Polynya, leading to an unprecedented input of marine planktonic and sea ice-related diatoms at RICE and low dust influx, in tandem with decreased snow accumulation and increased sea-ice extent in the ERS/Amundsen Sea. We propose that the increased efficiency of the polynya during the period covering the Little Ice Age is related to the eastward expansion of the Ross Sea Polynya and Roosevelt Island polynya formation, which extends as a protrusion of the much larger Ross Sea polynya, but with a significant regional impact in the Ross Sea area.

FIGURES AND FIGURE CAPTIONS

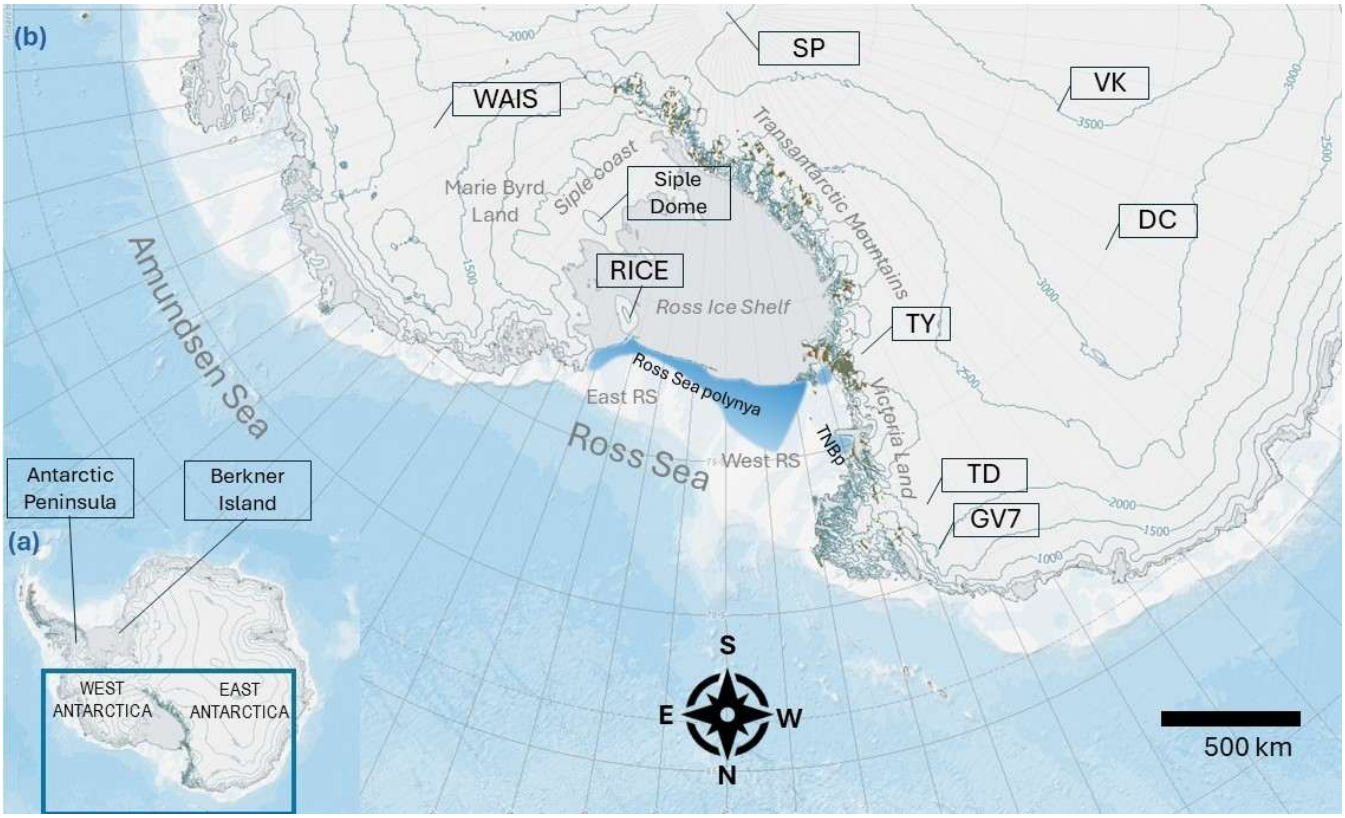

Fig. 1- Map of Antarctica with regions and drilling sites cited in the text (source: SCAR Antarctic Digital Database, https://add.scar.org/). East RS: Eastern Ross Sea; West RS: Western Ross Sea; SP: South Pole; DC: Dome C; VK: Vostok; TY: Taylor Dome; TD: Talos Dome. Blue shaded area (redrawn from Mezgec et al., 2017) represent the Ross Sea polynya, and the much smaller McMurdo Sound and Terra Nova Bay (TNBp) polynyas.

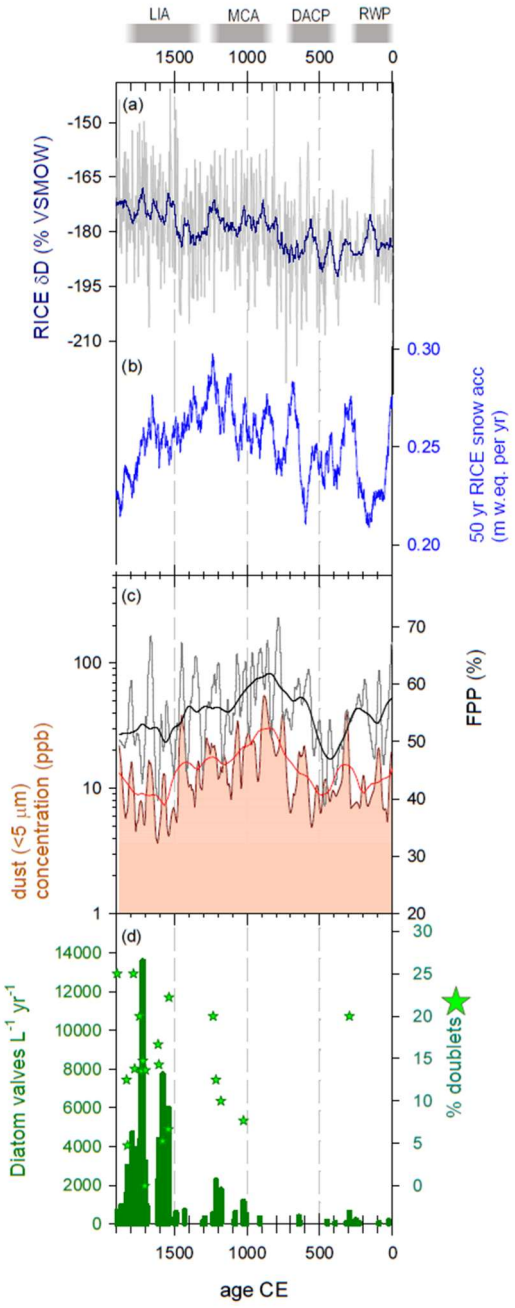
LIA
MCA
DACP
RWP
1500
1000
500
0
(a)
RICE δD (‰ VSMOW)
-150
-165
-180
-195
-210
(b)
0.30
0.25
0.20
50 yr RICE snow acc
(m w.eq. per yr)
(c)
100
10
1
dust (<5 μm)
concentration (ppb)
70
60
50
40
30
20
FPP (%)
(d)
14000
12000
10000
8000
6000
4000
2000
0
Diatom valves L-1 yr-1
30
25
20
15
10
5
0
% doublets
1500
1000
500
0
age CE

Fig. 2- The climate history of RICE over the past 2 kyr. RWP: Roman Warm Period; DACP: Dark Ages Cold Period; MCA: Medieval Climate Anomaly; LIA: Little Ice Age.

(a) RICE water stable isotope record (δD ‰VSMOW; blue line: 50-yrs running mean);

(b) Snow accumulation at the site (50-yrs running mean). (a) and (b) data from Bertler et al., 2018.

(c) Dust size index FPP (%) defined as in Delmonte et al. (2017), light grey. 20-yrs running mean and local smoothing (Loess, polynomial degree 1, sampling proportion 0.1), black. Concentration (log) of dust particles smaller than 5 μm, dark red. 20-yrs running mean and Loess local smoothing as in (c), red.

(d) Diatom content of samples, expressed as number of diatom valves per Liter per year. Green stars indicate the percentage of doublets in the samples.

Plots (c) and (d) are generated from data obtained in this work; these are reported in Supplementary Tables ST1 and ST2.

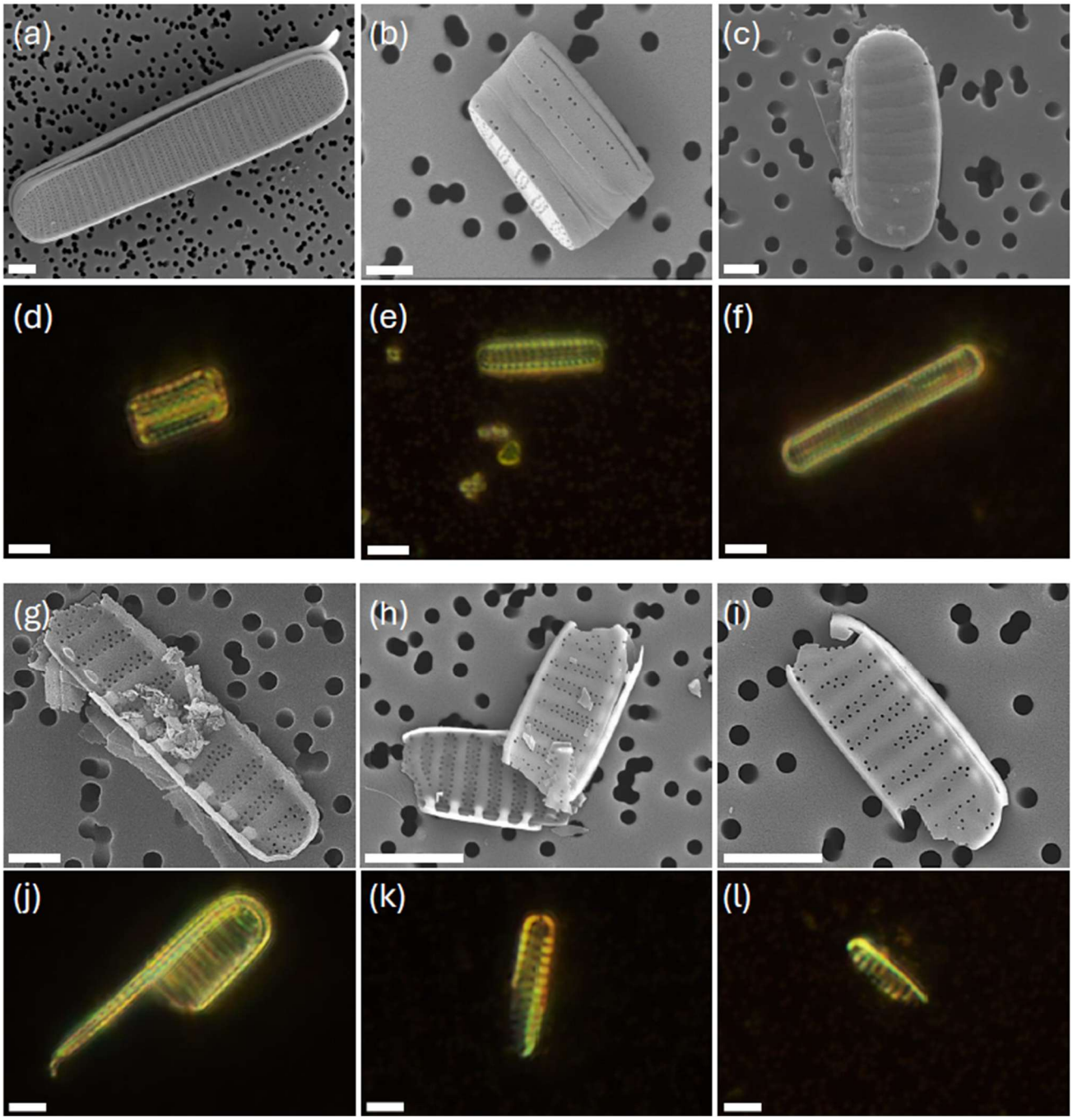

Fig. 3- Scanning Electron Microscope (a, b, c, g, h, i) and optical microscope (d, e, f, j, k, l) images of entire diatom valves (a to f) and valve fragments (g to l). Scale bar: 1 µm for SEM images and 5 µm for optical images (magnification 1000x).

600

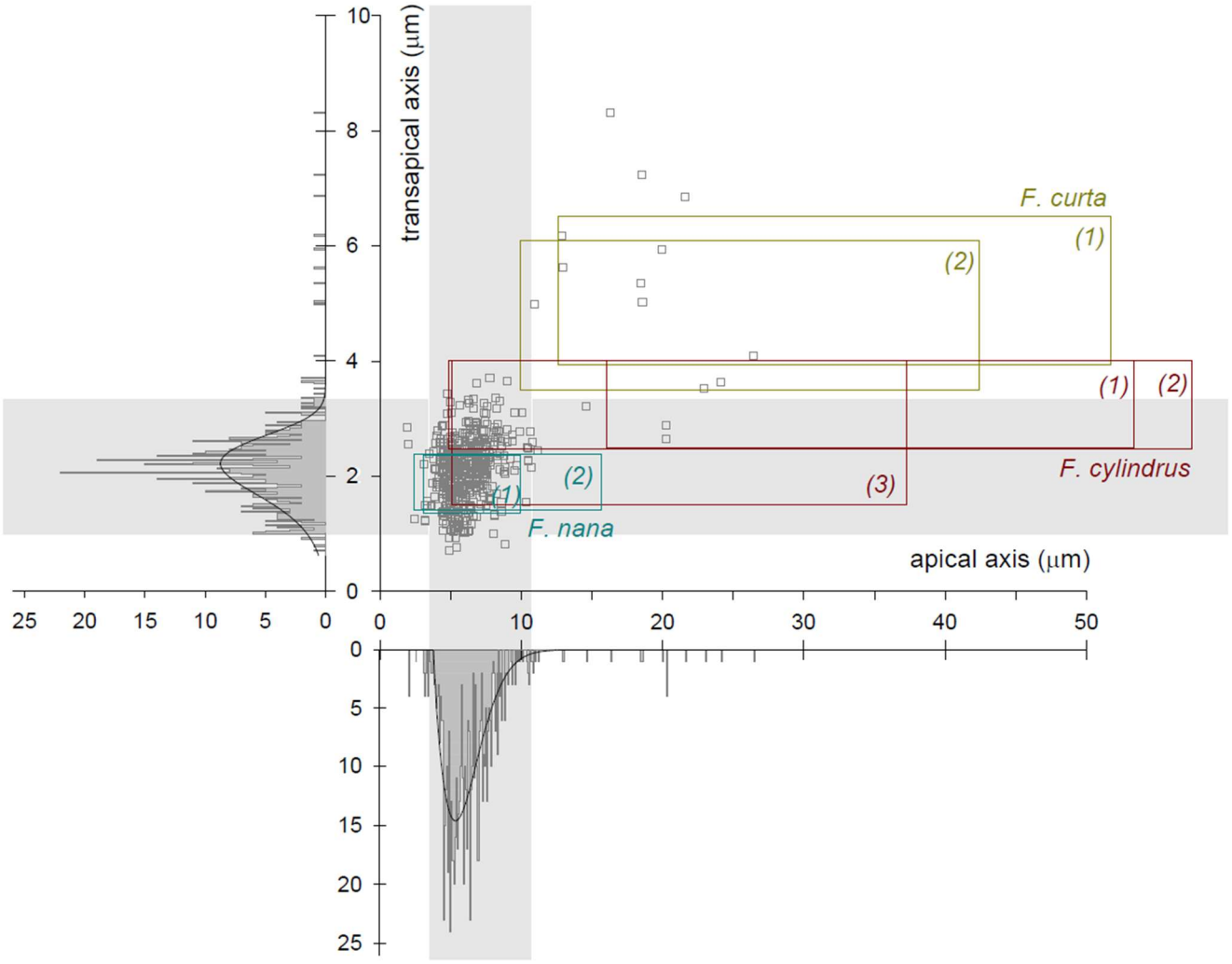

Fig. 4- Morphometric data of entire valves from the RICE ice core. Apical axis (µm) vs transapical axis (µm). Frequency histograms (bottom and left) are also reported. Grey bands indicate the interval where 95% of specimens are included. Boxes with n.1 refer to morphometric data for *F.cylindrus, F.nana, F.curta* from Cefarelli et al., 2010; boxes marked with n.2 refer to earlier literature morphometric data collected and listed in Cefarelli et al., 2010. Box with n. 3 refers to data from Lundholm and Hasle (2008) for *F.cylindrus*.

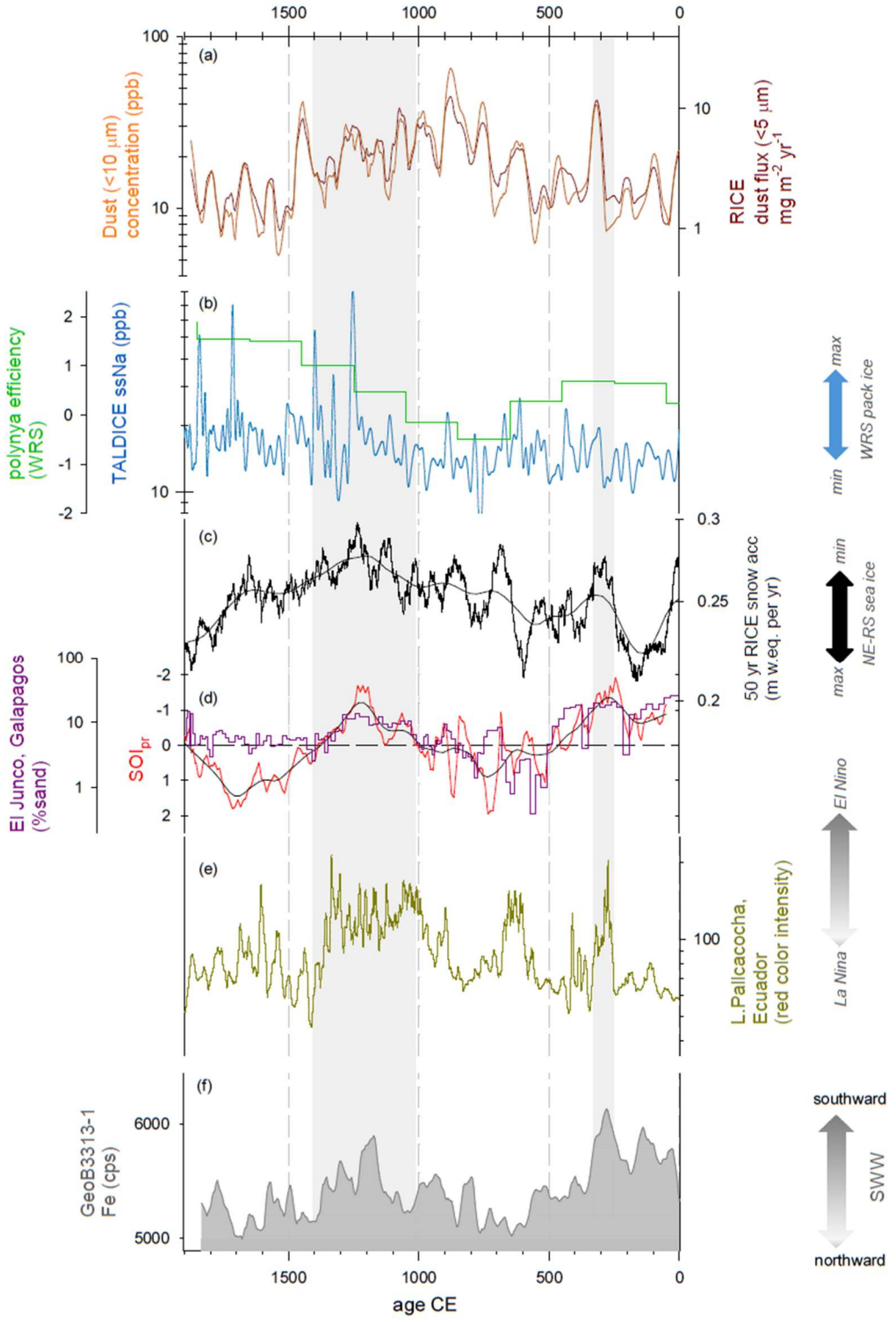
1500
1000
500
0
(a)
Dust (<10 μm) concentration (ppb)
RICE dust flux (<5 μm) mg m-2 yr-1
(b)
polynya efficiency (WRS)
TALDICE ssNa (ppb)
max
min
WRS pack ice
(c)
50 yr RICE snow acc (m w.eq. per yr)
min
max
NE-RS sea ice
(d)
El Junco, Galapagos (%sand)
SOIpr
El Nino
La Nina
(e)
L.Pallcacocha, Ecuador (red color intensity)
(f)
GeoB3313-1 Fe (cps)
southward
SWW
northward
age CE

Fig. 5- Comparison of ice core and climate records from the Southern Hemisphere over the last 2000 years. (a) RICE concentration of dust particles smaller than 10 µm (ppb), and RICE flux (mg m^{-2} $year^{-1}$) of particles smaller than 5 µm (30-year running average). (b) Sea salt Sodium (ssNa) concentration at TALDICE (and polynya efficiency (Mezgec et al., 2017). (c) RICE snow accumulation rate, as in fig. 2b. (d) Red line: Southern Oscillation Index (SOI_{pr}) record (with Loess smooth superposed, black line) from Yan et al. (2011). This index was calculated as the difference between the reconstructed precipitation records from Indonesia and the Galapagos (see text). Purple line: rainfall history of the Galapagos, used in the reconstruction of SOIpr, but extending on a longer time period. This series is derived from a lake level reconstruction based on grain size data from Lago El Junco sediment core. (e) Laguna Pallcacocha (Ecuador) red color intensity record of sediments (Moy et al., 2022, 30-years running average). El Niño-related high precipitation events are related to greater colour intensities. (f) Iron content from GeoB3313-1 core smoothed over a 20-year running average (Lamy et al., 2001); higher Fe concentrations indicate a poleward position of the South Westerly Winds (SWW) and vice versa.

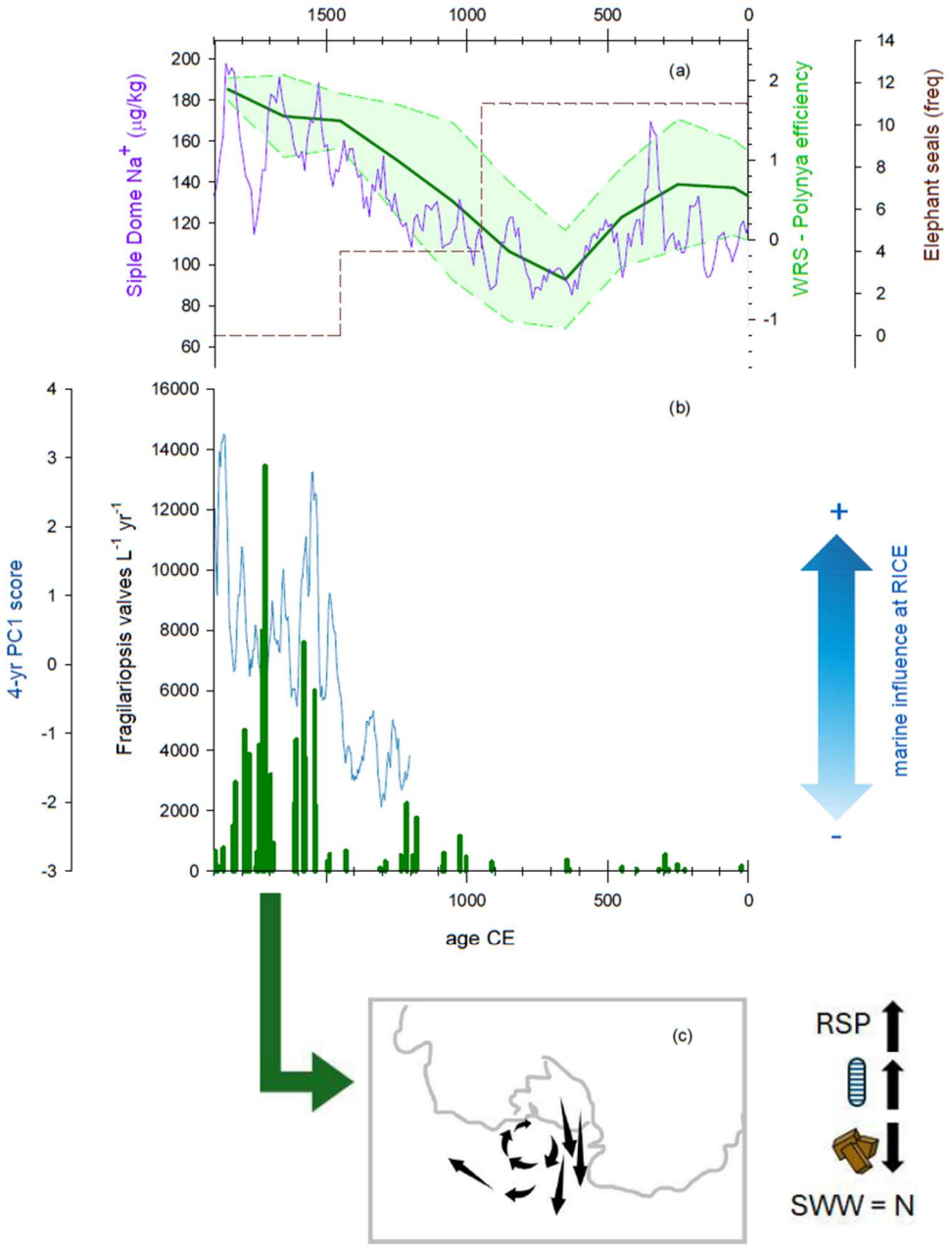

Fig. 6- (a) Polynya efficiency (Mezgec et al., 2017) with standard deviation values, derived from a stacked record of *F. curta* from the landfast sea ice zone of the Western Ross Sea and ssNa record from Taylor Dome (see Mezgec et al., 2017 for details). Elephant seal frequency data from Hall et al., 2006 (as reported in Mezgec et al., 2017). Sodium data from Siple Dome are also reported (Kreutz et al., 1997) (b) First principal component obtained from the 4 year-resolved ICP-MS data series

(Brightley, 2017) spanning the period 1204-1992 CE; PC1 explains 62% of the variance and is related to marine-sourced winds (see text). Green histograms refer to the number of entire *Fragilariopsis* spp. valves per Liter per year (same as in fig. SF5 c). (c) Qualitative sketch of the atmospheric circulation pattern leading to expansion of the Ross Sea polynya and diatom transport to RICE. Arrows on the right show expansion of the Ross Sea polynya, increase in aeolian diatom content, decrease in dust influx and northward shift of the south Westerlies.

Data availability

Dust and diatom data generated in this study are included in the Supplement as Table S1 and Table S2, respectively.

Supplement

The supplement related to this article is available online at XXX

Author contributions

SL and BD designed the study and conducted the dust and diatom analysis. GB contributed to ice core sample cutting and dust analysis. SL, DT and EM conducted the interpretation of diatom data. NB provided the ice core samples. SL and BD conducted the interpretation of all dust, diatom and paleoclimate data reported in this study and wrote the first draft of the article. All co-authors contributed to data interpretation and provided important edits and comments on subsequent drafts.

Competing interests

The contact author has declared that none of the authors has any competing interests.

Acknowledgements

This work is a contribution to the Roosevelt Island Climate Evolution (RICE) Program, funded by national contributions from New Zealand, Australia, Denmark, Germany, Italy, the People's Republic of China, Sweden, the UK and the USA. Logistics support was provided by Antarctica New Zealand (K049) and the US Antarctic Program. This article is an outcome of Progetto TECLA - Dipartimenti di Eccellenza 2023–2027, funded by MUR. We also acknowledge funding to support the collecting of the RICE ice core and analysis of isotope and geochemical records through the NZ Ministry of Business, Innovation and Employment (15-VUW-131, RDF-VUW1103) and GNS Science (Global Change through Time, 540GCT12).

We thank Claudio Artoni for support in the EUROCOLD laboratory, and Sofia Cerri for helping in diatom slide preparation and dust analyses.

Financial support

Funding provided by MIUR – Dipartimenti di Eccellenza 2023–2027, Project TECLA, Department of Earth and Environmental Sciences, University of Milano-Bicocca.

References

Allen, C. S., Thomas, E. R., Blagbrough, H., Tetzner, D. R., Warren, R. A., Ludlow, E. C., and Bracegirdle, T. J.: Preliminary evidence for the role played by South Westerly wind strength on the marine diatom content of an Antarctic Peninsula Ice Core (1980–2010), Geosci., 10, 87, https://doi.org/10.3390/geosciences10030087, 2020.

Arrigo, K. R. and van Dijken, G. L.: Phytoplankton dynamics within 37 Antarctic coastal polynya systems, J. Geophys. Res.-Oceans, 108, https://doi.org/10.1029/2002JC001739, 2003.

Bertler, N. A. N., Barrett, P. J., Mayewski, P. A., Fogt, R. L., Kreutz, K. J., and Shulmeister, J.: El Niño suppresses Antarctic warming, Geophys. Res. Lett., 31, L15207, https://doi.org/10.1029/2004GL020749, 2004.

Bertler, N. A. N., Naish, T. R., Mayewski, P. A., and Barrett, P. J.: Opposing oceanic and atmospheric ENSO influences on the Ross Sea Region, Antarctica, Adv. Geosci., 6, 83–86, https://doi.org/10.5194/adgeo-6-83-2006, 2006.

Bertler, N. A. N., Mayewski, P. A., and Carter, L.: Cold conditions in Antarctica during the Little Ice Age – Implications for abrupt climate change mechanisms, Earth Planet. Sci. Lett., 308, 41–51, https://doi.org/10.1016/j.epsl.2011.05.021, 2011.

Bertler, N. A. N., Conway, H., Dahl-Jensen, D., Emanuelsson, D. B., Winstrup, M., Vallelonga, P. T., Lee, J. E., Brook, E. J., Severinghaus, J. P., Fudge, T. J., Keller, E. D., Baisden, W. T., Hindmarsh, R. C. A., Neff, P. D., Blunier, T., Edwards, R., Mayewski, P. A., Kipfstuhl, S., Buizert, C., Canessa, S., Dadic, R., Kjær, H. A., Kurbatov, A., Zhang, D., Waddington, E. D., Baccolo, G., Beers, T., Brightley, H. J., Carter, L., Clemens-Sewall, D., Ciobanu, V. G., Delmonte, B., Eling, L., Ellis, A., Ganesh, S., Golledge, N. R., Haines, S., Handley, M., Hawley, R. L., Hogan, C. M., Johnson, K. M., Korotkikh, E., Lowry, D. P., Mandeno, D., McKay, R. M., Menking, J. A., Naish, T. R., Noerling, C., Ollive, A., Orsi, A., Proemse, B. C., Pyne, A. R., Pyne, R. L., Renwick, J., Scherer, R. P., Semper, S., Simonsen, M., Sneed, S. B., Steig, E. J., Tuohy, A., Venugopal, A. U.,

Valero-Delgado, F., Venkatesh, J., Wang, F., Wang, S., Winski, D. A., Winton, V. H. L., Whiteford, A., Xiao, C., Yang, J., and Zhang, X.: The Ross Sea Dipole – temperature, snow accumulation and sea ice variability in the Ross Sea region, Antarctica, over the past 2700 years, Clim. Past, 14, 193–214, https://doi.org/10.5194/cp-14-193-2018, 2018.

Bory, A., Biscaye, P. E., Piotrowski, A. M., and Steffensen, J. P.: Multiple sources supply aeolian mineral dust to the Atlantic sector of coastal Antarctica: Evidence from recent snow layers at the top of Berkner Island ice sheet, Earth Planet. Sci. Lett., 291, 138–148, https://doi.org/10.1016/j.epsl.2010.01.006, 2010.

Bradley, R. S., Hughes, M. K., and Diaz, H. F.: Climate in medieval time, Science, 302, 404–405, https://doi.org/10.1126/science.1090372, 2003.

Brightley, H. J.: A Paleoclimate Reconstruction of the Little Ice Age to Modern Era Climate Conditions in the Eastern Ross Sea, Antarctica as Captured in the RICE Ice Core. MSc thesis, Victoria University of Wellington, Wellington, New Zealand, 2017.

Bromwich, D. H. and Robasky, F. M.: Recent precipitation trends over the polar ice sheets, Meteorol. Atmos. Phys., 51, 259–274, https://doi.org/10.1007/BF01030498, 1993.

Bromwich, D., Liu, Z., Rogers, A. N., and Van Woert, M. L.: Winter atmospheric forcing of the Ross Sea polynya, in: Ocean, Ice and Atmosphere: Interactions at the Antarctic Continental Margin, edited by: Jacobs, S. S. and Weiss, R. F., Antarct. Res. Ser., 75, AGU, Washington, DC, 101–133, https://doi.org/10.1029/AR075p0101, 1998.

Burckle, L. H., Gayley, R. I., Ram, M., and Lille, R. J.: Diatoms in Antarctic ice cores: Some implications for the glacial history of Antarctica, Geology, 16, 326–329, https://doi.org/10.1130/0091-7613(1988)016%3C0326:DIAICS%3E2.3.CO;2, 1988.

Caiazzo, L., Baccolo, G., Barbante, C., Becagli, S., Bertò, M., Ciardini, V., Crotti, I., Delmonte, B., Dreossi, G., Frezzotti, Gabrieli, J., Giardi, F., Han, Y., Hong, S. -B., Hur, S. D., Hwang, H., Kang, J. -H., Narcisi, B., Proposito, M., Scarchilli, C., M., Selmo, E., Severi, M., Spolaor, A., Stenni, B., Traversi, R., and Udisti, R.: Prominent features in isotopic, chemical and dust stratigraphies from coastal East Antarctic ice sheet (Eastern Wilkes Land), Chemosphere, 176, 273–287, https://doi.org/10.1016/j.chemosphere.2017.02.115, 2017.

Carrasco, J. F., Bromwich, D. H., and Monaghan, A. J.: Distribution and characteristics of mesoscale cyclones in the Antarctic: Ross Sea eastward to the Weddell Sea, Mon. Weather Rev., 131, 289–301, https://doi.org/10.1175/1520-0493(2003)131<0289:DACOMC>2.0.CO;2, 2003.

Cefarelli, A. O., Ferrario, M. E., Almandoz, G. O., Atencio, A. G., Akselman, R., and Vernet, M.: Diversity of the diatom genus Fragilariopsis in the Argentine Sea and Antarctic waters: morphology, distribution and abundance, Polar Biol., 33, 1463–1484, https://doi.org/10.1007/s00300-010-0794-z, 2010.

Delmonte, B., Baroni, C., Andersson, P. S., Narcisi, B., Salvatore, M. C., Petit, J. R., Scarchilli, C., Frezzotti, M., Albani, S., and Maggi, V.: Modern and Holocene aeolian dust variability from Talos Dome (Northern Victoria Land) to the interior of the Antarctic ice sheet, Quat. Sci. Rev., 64, 76–89, https://doi.org/10.1016/j.quascirev.2012.11.033, 2013.

Delmonte, B., Paleari, C. I., Andò, S., Garzanti, E., Andersson, P. S., Petit, J. R., Crosta, X., Narcisi, B., Baroni, C., Salvatore, M. C., Baccolo, G., and Maggi, V.: Causes of dust size variability in central East Antarctica (Dome B): Atmospheric transport from expanded South American sources during Marine Isotope Stage 2, Quat. Sci. Rev., 168, 55–68, https://doi.org/10.1016/j.quascirev.2017.05.009, 2017.

Delmonte, B., Winton, H., Baroni, M., Baccolo, G., Hansson, M., Andersson, P., Baroni, C., Salvatore, M. C., Lanci, L., and Maggi, V.: Holocene dust in East Antarctica: Provenance and variability in time and space, Holocene, 30, 546–558, https://doi.org/10.1177/0959683619875188, 2020.

Drucker, R., Martin, S., and Kwok, R.: Sea ice production and export from coastal polynyas in the Weddell and Ross Seas, Geophys. Res. Lett., 38, L17502, https://doi.org/10.1029/2011GL048668, 2011.

Emanuelsson, B. D.: Central tropical Pacific ENSO variability preserved in water stable isotopes from the Roosevelt Island Climate Evolution (RICE) ice core, Antarctica. High-Resolution Water Stable Isotope Ice-Core Record: Roosevelt Island, Antarctica PhD Thesis, 143 pp., 2016.

Emanuelsson, B. D., Bertler, N. A. N., Neff, P. D., Renwick, J. A., Markle, B. R., Baisden, W. T., and Keller, E. D.: The role of Amundsen–Bellingshausen Sea anticyclonic circulation in forcing marine air intrusions into West Antarctica, Clim. Dyn., 51, 3579–3596, https://doi.org/10.1007/s00382-018-4097-3, 2018.

Emanuelsson, B. D., Renwick, J. A., Bertler, N. A. N., Baisden, W. T., Thomas, E. R.: The role of large-scale drivers in the Amundsen Sea Low variability and associated changes in water isotopes from the Roosevelt Island ice core, Antarctica, Clim. Dyn., 60, 4145–4155, https://doi.org/10.1007/s00382-022-06589-2, 2023.

Fraser, A. D., Ohshima, K. I., Nihashi, S., Massom, R. A., Tamura, T., Nakata, K., Williams, G. D., Carpentier, S., and Willmes, S.: Landfast ice controls on sea-ice production in the Cape Darnley Polynya: A case study, Remote Sens. Environ., 233, 111315, https://doi.org/10.1016/j.rse.2019.111315, 2019.

Fusco, G., Budillon, G., and Spezie, G.: Surface heat fluxes and thermohaline variability in the Ross Sea and in Terra Nova Bay polynya, Cont. Shelf Res., 29, 1887–1895, https://doi.org/10.1016/j.csr.2009.07.006, 2009.

Hall, B. L., Hoelzel, A. R., Baroni, C., Denton, G. H., Le Boeuf, B. J., Overturf, B., and Töpf, A. L.: Holocene elephant seal distribution implies warmer-than-present climate in the Ross Sea, P. Natl. Acad. Sci. USA, 103, 10213–10217, https://doi.org/10.1073/pnas.0604002103, 2006.

Hall, B. L., Koch, P. L., Baroni, C., Salvatore, M. C., Hoelzel, A. R., de Bruyn, M., and Welch, A. J.: Widespread southern elephant seal occupation of the Victoria land coast implies a warmer-than-present Ross Sea in the mid-to-late Holocene, Quat. Sci. Rev., 303, 107991, https://doi.org/10.1016/j.quascirev.2023.107991, 2023.

Helama, S., Jones, P. D., and Briffa, K. R.: Dark Ages Cold Period: A literature review and directions for future research, Holocene, 27, 1600–1606, https://doi.org/10.1177/0959683617693898, 2017.

Heinemann, G., and Klein, T.: Simulations of topographically forced mesocyclones in the Weddell Sea and the Ross Sea region of Antarctica, Mon. Weather Rev., 131, 302–316, https://doi.org/10.1175/1520-0493(2003)131<0302:SOTFMI>2.0.CO;2, 2003.

IPCC, 2021: *Climate Change 2021: The Physical Science Basis. Contribution of Working Group I to the Sixth Assessment Report of the Intergovernmental Panel on Climate Change* Masson-Delmotte, V., Zhai, P., Pirani, A., Connors, S. L., Péan, C., Berger, S., Caud, N., Chen, Y., Goldfarb, L., Gomis, M. I., Huang, M., Leitzell, K., Lonnoy, E., Matthews, J. B. R., Maycock, T. K., Waterfield, T., Yelekçi, O., Yu, R., and Zhou, B.: Climate Change 2021: The Physical Science Basis. Contribution of Working Group I to the Sixth Assessment Report of the Intergovernmental Panel on Climate Change. Cambridge University Press, Cambridge, United Kingdom and New York, NY, USA, IPPC, 2391, https://doi.org/10.1017/9781009157896, 2021.

Jacobs, S. S., and Comiso, J. C.: Sea ice and oceanic processes on the Ross Sea continental shelf, J. Geophys. Res.-Oceans, 94, 18195–18211, https://doi.org/10.1029/JC094iC12p18195, 1989.

Jones, P. D., and Mann, M. E.: Climate over past millennia, Rev. Geophys., 42, RG2002, https://doi.org/10.1029/2003RG000143, 2004.

Kellogg, D. E., and Kellogg, T. B.: Diatoms in South Pole ice: Implications for aeolian contamination of Sirius Group deposits, Geology, 24, 115–118, https://doi.org/10.1130/0091-7613(1996)024<0115:DISPII>2.3.CO;2, 1996.

Kellogg, D. E., and Kellogg, T. B.: Frozen in time: The diatom record in ice cores from remote drilling sites on the Antarctic ice sheets, in: Antarctic Research Series, Princeton University Press, Princeton, NJ, USA, 69–93, 2005.

Kingslake, J., Hindmarsh, R. C. A., Aðalgeirsdóttir, G., Conway, H., Corr, H. F. J., Gillet-Chaulet, F., Martín, C., King, E. C., Mulvaney, R., and Pritchard, H. D.: Full-depth englacial vertical ice sheet velocities measured using phase-sensitive radar, J. Geophys. Res.-Earth Surf., 119, 2604–2618, https://doi.org/10.1002/2014JF003275, 2014.

Klein, T., and Heinemann, G.: On the forcing mechanisms of mesocyclones in the eastern Weddell Sea region, Antarctica: Process studies using a mesoscale numerical model, Meteorol. Z., 10, 113–122, https://doi.org/10.1127/0941-2948/2001/0010-0113, 2001.

Koffman, B. G., Kreutz, K. J., Breton, D. J., Kane, E. J., Winski, D. A., Birkel, S. D., Kurbatov, A. V., and Handley, M. J.: Centennial-scale variability of the Southern Hemisphere westerly wind belt in the eastern Pacific over the past two millennia, Clim. Past, 10, 1125–1144, https://doi.org/10.5194/cp-10-1125-2014, 2014.

Kreutz, K. J., Mayewski, P. A., Meeker, L. D., Twickler, M. S., Whitlow, S. I., and Pittalwala, I. I.: Bipolar changes in atmospheric circulation during the Little Ice Age, Science, 277, 12941296, 1997.

Lamb, H. H.: The early medieval warm epoch and its sequel, Palaeogeogr. Palaeoclimatol. Palaeoecol., 1, 13–37, https://doi.org/10.1016/0031-0182(65)90004-0, 1965.

Lamy, F., Hebbeln, D., Röhl, U., and Wefer, G.: Holocene rainfall variability in southern Chile: a marine record of latitudinal shifts of the Southern Westerlies, Earth Planet. Sc. Lett., 185, 369–382, https://doi.org/10.1016/S0012-821X(00)00381-2, 2001.

Lee, J. E., Brook, E. J., Bertler, N. A. N., Buizert, C., Baisden, T., Blunier, T., Ciobanu, V. G., Conway, H., Dahl-Jensen, D., Fudge, T. J., Hindmarsh, R., Keller, E. D., Parrenin, F., Severinghaus, J. P., Vallelonga, P., Waddington, E. D., and Winstrup, M.: An 83 000-year-old ice core from Roosevelt Island, Ross Sea, Antarctica, Clim. Past, 16, 1691–1713, https://doi.org/10.5194/cp-16-1691-2020, 2020.

Legrand, M., and Kirchner, S.: Polar atmospheric circulation and chemistry of recent (1957-1983) south polar precipitation, Geophys. Res. Lett., 15, 879–882, https://doi.org/10.1029/GL015i008p00879, 1988.

Li, X., Cai, W., Meehl, G. A., Chen, D., Yuan, X., Raphael, M., Holland, D. M., Ding, Q., Fogt, R. L., Markle, B. R., Wang, G., Bromwich, D. H., Turner, J., Xie, S.-P., Steig, E. J., Gille, S. T., Xiao, C., Wu, B., Lazzara, M. A., Chen, X., Stammerjohn, S., Holland, P. R., Holland, M. M., Cheng, X., Price, S. F., Wang, Z., Bitz, C. M., Shi, J., Gerber, E. P., Liang, X., Goosse, H., Yoo, C., Ding, M., Geng, L., Xin, M., Li, C., Dou, T., Liu, C., Sun, W., Wang, X., and Song, C.: Tropical teleconnection impacts on Antarctic climate changes, Nat. Rev. Earth Environ., 2, 680–698, https://doi.org/10.1038/s43017-021-00204-5, 2021.

Ljungqvist, F. C.: A new reconstruction of temperature variability in the extra-tropical Northern Hemisphere during the last two millennia, Geogr. Ann. Ser. A-Phys. Geogr., 92, 339–351, https://doi.org/10.1111/j.1468-0459.2010.00399.x, 2010.

Lundholm, N., and Hasle, G. R.: Are Fragilariopsis cylindrus and Fragilariopsis nana bipolar diatoms?–Morphological and molecular analyses of two sympatric species. Nova Hedwigia, Beiheft, 133, 231-250, 2008.

Macha, J. M. A., Mackintosh, A. N., McCormack, F. S., Henley, B. J., McGregor, H. V., Van Dalum, C. T., & Purich, A.: Distinct Central and Eastern Pacific El Niño Influence on Antarctic Surface Mass Balance. *Geophysical Research Letters*, *51*(11), e2024GL109423, https://doi.org/10.1029/2024GL109423, 2024.

Maffezzoli, N., Cook, E., van der Bilt, W. G. M., Støren, E. N., Festi, D., Muthreich, F., Seddon, A. W. R., Burgay, F., Baccolo, G., Mygind, A. R. F., Petersen, T., Spolaor, A., Vascon, S., Pelillo, M., Ferretti, P., dos Reis, R. S., Simões, J. C., Ronen, Y., Delmonte, B., Viccaro, M., Steffensen, J. P., Dahl-Jensen, D., Nisancioglu, K. H., and Barbante, C.: Detection of ice core particles via deep neural networks, The Cryosphere, 17, 539–565, https://doi.org/10.5194/tc-17-539-2023, 2023.

Mann, M. E., Zhang, Z., Rutherford, S., Bradley, R. S., Hughes, M. K., Shindell, D., Ammann, C., Faluvegi, G., and Ni, F.: Global signatures and dynamical origins of the Little Ice Age and Medieval Climate Anomaly, Science, 326, 1256–1260, https://doi.org/10.1126/science.1177303, 2009.

Masson, V., Vimeux, F., Jouzel, J., Morgan, V., Delmotte, M., Ciais, P., Hammer, C., Johnsen, S., Lipenkov, V. Ya., Mosley-Thompson, E., Petit, J. R., Steig, E. J., Stievenard, M., and Vaikmae, R.: Holocene climate variability in Antarctica based on 11 ice-core isotopic records, Quat. Res., 54, 348–358, https://doi.org/10.1006/qres.2000.2172, 2000.

Matthews, J. A., and Briffa, K. R.: The 'Little Ice Age': re-evaluation of an evolving concept, Geogr. Ann. Ser. A-Phys. Geogr., 87, 17–36, https://doi.org/10.1111/j.0435-3676.2005.00242.x, 2005.

McKay, R. M., Barrett, P. J., Harper, M. A., and Hannah, M. J.: Atmospheric transport and concentration of diatoms in surficial and glacial sediments of the Allan Hills, Transantarctic Mountains, Palaeogeogr. Palaeoclimatol. Palaeoecol., 260, 168–183, https://doi.org/10.1016/j.palaeo.2007.08.014, 2008.

Mezgec, K., Stenni, B., Crosta, X., Masson-Delmotte, V., Baroni, C., Braida, M., Ciardini, V., Colizza, E., Melis, R., Salvatore, M. C., Severi, M., Scarchilli, C., Traversi, R., Udisti, R., and Frezzotti, M.: Holocene sea ice variability driven by wind and polynya efficiency in the Ross Sea, Nat. Commun., 8, 1334, https://doi.org/10.1038/s41467-017-01455-x, 2017.

Morales Maqueda, M. A., Willmott, A. J., and Biggs, N. R. T.: Polynya dynamics: a review of observations and modeling, Rev. Geophys., 42, RG1004, https://doi.org/10.1029/2002RG000116, 2004.

Moy, C. M., Seltzer, G. O., Rodbell, D. T., and Anderson, D. M.: Variability of El Niño/Southern Oscillation activity at millennial timescales during the Holocene epoch, Nature, 420, 162–165, https://doi.org/10.1038/nature01194, 2002.

Neff, P. D., and Bertler, N. A. N.: Trajectory modeling of modern dust transport to the Southern Ocean and Antarctica, J. Geophys. Res.-Atmos., 120, 9303–9322, https://doi.org/10.1002/2015JD023304, 2015.

O'Connor, G.K., Steig, E.J. and Hakim, G.J.: Strengthening Southern Hemisphere westerlies and Amundsen Sea low deepening over the 20th century revealed by proxy-data assimilation, Geophys. Res. Let., 48, e2021GL095999, https://doi.org/10.1029/2021GL095999, 2021.

PAGES2k Consortium: A global multiproxy database for temperature reconstructions of the Common Era, Scientific data, 4, 170088, https://doi.org/10.1038/sdata.2017.88, 2017.

Park, J., Kim, H.-C., Kidwell, A., and Hwang, J.: Multi-temporal variation of the Ross Sea Polynya in response to climate forcings, Polar Res., 37, 1444891, https://doi.org/10.1080/17518369.2018.1444891, 2018.

Petit, J.-R., and Delmonte, B.: A model for large glacial–interglacial climate-induced changes in dust and sea salt concentrations in deep ice cores (central Antarctica): palaeoclimatic implications and prospects for refining ice core chronologies, Tellus B, 61, 768–790, https://doi.org/10.1111/j.1600-0889.2009.00463.x, 2009.

Raphael, M. N., Holland, M. M., Landrum, L., and Hobbs, W. R.: Links between the Amundsen Sea Low and sea ice in the Ross Sea: seasonal and interannual relationships, Clim. Dyn., 52, 2333–2349, https://doi.org/10.1007/s00382-018-4258-4, 2019.

Rein, B., Lückge, A., Reinhardt, L., Sirocko, F., Wolf, A., Dullo, W.-C.: El Niño variability off Peru during the last 20,000 years, Paleoceanogr. Paleoclimat., 20, https://doi.org/10.1029/2004PA001099, 2005.

Renwick, J. A.: ENSO-related variability in the frequency of South Pacific blocking. Monthly Weather Review 126.12: 3117-3123. 1998.

Rhodes, R. H., Bertler, N. A. N., Baker, J. A., Steen-Larsen, H. C., Sneed, S. B., Morgenstern, U., and Johnsen, S. J.: Little Ice Age climate and oceanic conditions of the Ross Sea, Antarctica from a coastal ice core record, Clim. Past, 8, 1223–1238, https://doi.org/10.5194/cp-8-1223-2012, 2012.

Sinclair, K. E., Bertler, N. A. N., and Trompetter, W. J.: Synoptic controls on precipitation pathways and snow delivery to high-accumulation ice core sites in the Ross Sea region, Antarctica, J. Geophys. Res.-Atmos., 115, D22112, https://doi.org/10.1029/2010JD014383, 2010.

Smerdon, J. E., and Pollack, H. N.: Reconstructing Earth's surface temperature over the past 2000 years: the science behind the headlines, Wiley Interdiscip. Rev.-Clim. Change, 7, 746–771, https://doi.org/10.1002/wcc.418, 2016.

Steig, E. J., Morse, D. L., Waddington, E. D., Stuiver, M., Grootes, P. M., Mayewski, P. A., Twickler, M. S., and Whitlow, S. I.: Wisconsinan and holocene climate history from an ice core at taylor dome, western ross embayment, antarctica, Geogr. Ann. Ser. A-Phys. Geogr., 82, 213–235, https://doi.org/10.1111/j.0435-3676.2000.00122.x, 2000.

Stenni, B., Curran, M. A. J., Abram, N. J., Orsi, A., Goursaud, S., Masson-Delmotte, V., Neukom, R., Goosse, H., Divine, D., van Ommen, T., Steig, E. J., Dixon, D. A., Thomas, E. R., Bertler, N. A. N., Isaksson, E., Ekaykin, A., Werner, M., and Frezzotti, M.: Antarctic climate variability on regional and continental scales over the last 2000 years, Clim. Past, 13, 1609–1634, https://doi.org/10.5194/cp-13-1609-2017, 2017.

Stenni, B., Buiron, D., Frezzotti, M., Albani, S., Barbante, C., Bard, E., Barnola, J. M., Baroni, M., Baumgartner, M., Bonazza, M., Capron, E., Castellano, E., Chappellaz, J., Delmonte, B., Falourd, S., Genoni, L., Iacumin, P., Jouzel, J., Kipfstuhl, S., Landais, A., Lemieux-Dudon, B., Maggi, V., Masson-Delmotte, V., Mazzola, C., Minster, B., Montagnat, M., Mulvaney, R., Narcisi, B., Oerter, H., Parrenin, F., Petit, J. R., Ritz, C., Scarchilli, C., Schilt, A., Schüpbach, S., Schwander, J., Selmo, E., Severi, M., Stocker, T. F., and Udisti, R.: Expression of the bipolar see-saw in Antarctic climate records during the last deglaciation, Nat. Geosci., 4, 46–49, https://doi.org/10.1038/ngeo1026, 2011.

Tesi, T., Belt, S. T., Gariboldi, K., Muschitiello, F., Smik, L., Finocchiaro, F., Giglio, F., Colizza, E., Gazzurra, G., Giordano, P., Morigi, C., Capotondi, L., Nogarotto, A., Köseoğlu, D., Di Roberto, A., Gallerani, A., Langone, L.: Resolving sea ice dynamics in the north-western Ross Sea during the last 2.6 ka: From seasonal to millennial timescales, Quat. Sci. Rev., 237, 106299, https://doi.org/10.1016/j.quascirev.2020.106299, 2020.

Tetzner, D. R., Thomas, E. R., and Allen, C.: Marine diatoms in ice cores from the Antarctic Peninsula and Ellsworth Land, Antarctica–species diversity and regional variability, The Cryosphere Discuss., 2021, 1–32, https://doi.org/10.5194/tc-2021-70, 2021.

Tetzner, D. R., Allen, C. S., and Thomas, E. R.: Regional variability of diatoms in ice cores from the Antarctic Peninsula and Ellsworth Land, Antarctica, The Cryosphere, 16, 779–798, https://doi.org/10.5194/tc-16-779-2022, 2022a.

Tetzner, D. R., Thomas, E. R., Allen, C. S., and Grieman, M. M.: Regional validation of the use of diatoms in ice cores from the Antarctic Peninsula as a Southern Hemisphere westerly wind proxy, Clim. Past, 18, 1709–1727, https://doi.org/10.5194/cp-18-1709-2022, 2022b.

Tuohy, A., Bertler, N. A. N., Neff, P. D., Edwards, R., Emanuelsson, D. B., Beers, T., and Mayewski, P. A.: Transport and deposition of heavy metals in the Ross Sea Region, Antarctica, J. Geophys. Res.-Atmos., 120, 10,996–11,011, https://doi.org/10.1002/2015JD023293, 2015.

Turner, J., Phillips, T., Hosking, J.S., Marshall, G.J. and Orr, A.: The Amundsen Sea Low, Int. J. Climat., 33, 1818–1829, https://doi.org/10.1002/joc.3558, 2013.

Turner, J., Hosking, J. S., Marshall, G. J., Phillips, T., Bracegirdle, T. L.: Antarctic sea ice increase consistent with intrinsic variability of the Amundsen Sea Low, Clim. Dyn., 46, 2391–2402, https://doi.org/10.1007/s00382-015-2708-9, 2016.

Tianjiao, W., Wei, H., and Xiao, J.: Dynamic linkage between the interannual variability of the spring Ross Ice Shelf Polynya and the atmospheric circulation anomalies, Clim. Dyn., 58, 831–840, https://doi.org/10.1007/s00382-021-05936-0, 2022.

Winstrup, M., Vallelonga, P., Kjær, H. A., Fudge, T. J., Lee, J. E., Riis, M. H., Edwards, R., Bertler, N. A. N., Blunier, T., Brook, E. J., Buizert, C., Ciobanu, G., Conway, H., Dahl-Jensen, D., Ellis, A., Emanuelsson, B. D., Hindmarsh, R. C. A., Keller, E. D., Kurbatov, A. V., Mayewski, P. A., Neff, P. D., Pyne, R. L., Simonsen, M. F., Svensson, A., Tuohy, A., Waddington, E. D., and Wheatley, S.: A 2700-year annual timescale and accumulation history for an ice core from Roosevelt Island, West Antarctica, Clim. Past, 15, 751–779, https://doi.org/10.5194/cp-15-751-2019, 2019.

Wang, T., Wei, H., & Xiao, J.: Dynamic linkage between the interannual variability of the spring Ross Ice Shelf Polynya and the atmospheric circulation anomalies. Climate Dynamics, 58(3), 831-840, https://doi.org/10.1007/s00382-021-05936-0, 2022.

Winton, V. H. L., Edwards, R., Delmonte, B., Ellis, A., Andersson, P. S., Bowie, A., Bertler, N. A. N., Neff, P., and Touhy, A.: Multiple sources of soluble atmospheric iron to Antarctic waters, Glob. Biogeochem. Cycles, 30, 421–437, https://doi.org/10.1002/2015GB005265, 2016a.

Winton, V. H. L., Dunbar, G. B., Atkins, C. B., Bertler, N. A. N., Delmonte, B., Andersson, P. S., Bowie, A., and Edwards, R.: The origin of lithogenic sediment in the south-western Ross Sea and implications for iron fertilization, Antarct. Sci., 28, 250–260, https://doi.org/10.1017/S0954102016000153, 2016b.

Wolff, E. W., Barbante, C., Becagli, S., Bigler, M., Boutron, C. F., Castellano, E., de Angelis, M., Federer, U., Fischer, H., Fundel, F., Hansson, M., Hutterli, M., Jonsell, U., Karlin, T., Kaufmann, P., Lambert, F., Littot, G. C., Mulvaney, R., Röthlisberger, R., Ruth, U., Severi, M., Siggaard-Andersen, M. L., Sime, L. C., Steffensen, J. P., Stocker, T. F., Traversi, R., Twarloh, B., Udisti, R., Wagenbach, D., and Wegner, A.: Changes in environment over the last 800,000 years from chemical analysis of the EPICA Dome C ice core, Quat. Sci. Rev., 29, 285–295, https://doi.org/10.1016/j.quascirev.2009.06.013, 2010.

Yan, H., Sun, L., Wang, Y., Huang, W., Qiu, S., and Yang, C.: A record of the Southern Oscillation Index for the past 2,000 years from precipitation proxies, Nat. Geosci., 4, 611–614, https://doi.org/10.1038/ngeo1231, 2011.

Yiu, Y. Y. S., and Maycock, A. C.: The linearity of the El Niño teleconnection to the Amundsen Sea region, Q. J. R. Meteorol. Soc., 146, 1196–1211, https://doi.org/10.1002/qj.3731, 2019.

Yokoyama, Y., Anderson, J. B., Yamane, M., Simkins, L. M., Miyairi, Y., Yamazaki, T., Koizumi, M., Suga, H., Kusahara, K., Prothro, L., Hasumi, H., Southon, J. R., and Ohkouchi, N.: Widespread collapse of the Ross Ice Shelf during the late Holocene, P. Natl. Acad. Sci. USA, 113, 2354–2359, https://doi.org/10.1073/pnas.1516908113, 2016.

Zhang, C., Li, T., and Li, S.: Impacts of CP and EP El Niño events on the Antarctic sea ice in austral spring, J. Clim., 34, 9327–9348, https://doi.org/10.1175/JCLI-D-21-0002.1, 2021.

Zwally, H. J., Comiso, J. C., and Gordon, A. L.: Antarctic offshore leads and polynyas and oceanographic effects, in: Oceanology of the Antarctic continental shelf, Antarct. Res. Ser., 43, 203–226, https://doi.org/10.1029/AR043p0203, 1985.